J. Fluid Mech. (2014), *vol.* 743, *pp.* 141–169. © Cambridge University Press 2014
doi:10.1017/jfm.2014.37

On Langmuir circulation in shallow waters

W. R. C. Phillips[1,3,†] **and A. Dai**[2,3]

[1]Department of Mathematics, Swinburne University of Technology, Hawthorn 3122, Australia

[2]Department of Water Resources and Environmental Engineering, Tamkang University, Taipei 25137, Taiwan

[3]Department of Theoretical and Applied Mechanics, University of Illinois at Urbana-Champaign, Urbana, IL 61801-2935, USA

(Received 4 October 2013; revised 12 January 2014; accepted 13 January 2014; first published online 4 March 2014)

The instability of shallow-water waves on a moderate shear to Langmuir circulation is considered. In such instances, specifically at the shallow end of the inner coastal region, the shear can significantly affect the drift giving rise to profiles markedly different from the simple Stokes drift. Since drift and shear are instrumental in the instability to Langmuir circulation, of key interest is how that variation in turn affects onset to Langmuir circulation. Also of interest is the effect on onset of various boundary conditions. To that end the initial value problem describing the wave–mean flow interaction which accounts for the multiple time scales of the surface waves, evolving shear and evolving Langmuir circulation is crafted from scratch, and includes the wave-induced drift and a consistent set of free-surface boundary conditions. The problem necessitates that Navier–Stokes be employed side by side with a set of mean-field equations. Specifically, the former is used to evaluate events with the shortest time scale, that is the wave field, while the mean field set is averaged over that time scale. This averaged set, the CLg equations, follow from the generalized Lagrangian mean equations and for the case at hand take the same form as the well-known CL equations, albeit with different time and velocity scales. Results based upon the Stokes drift are used as a reference to which those based upon drift profiles corrected for shear are compared, noting that the latter are asymptotic to the former as the waves transition from shallow to deep. Two typical temporal flow fields are considered: shear-driven flow and pressure-driven flow. Relative to the reference case, shear-driven flow is found to be destabilizing while pressure driven are stabilizing to Langmuir circulation. In pressure-driven flows it is further found that multiple layers, as opposed to a single layer, of Langmuir circulation can form, with the most intense circulations at the ocean floor. Moreover, the layers can extend into a region of flow beyond that in which the instability applies, suggesting that Langmuir circulation excited by the instability can in turn drive, as a dynamic consequence, contiguous albeit less intense Langmuir circulation. Pressure-driven flows also admit two preferred spacings, one closely in accord with observation for small-aspect-ratio Langmuir circulation, the other well in excess of observed large-aspect-ratio Langmuir circulation.

Key words: instability, shallow water flows, waves/free-surface flows

† Email address for correspondence: wrphilli@illinois.edu

Downloaded from https://www.cambridge.org/core. IFREMER - Brest, on 15 Jan 2017 at 17:03:33, subject to the Cambridge Core terms of use, available at https://www.cambridge.org/core/terms. https://doi.org/10.1017/jfm.2014.37

1. Introduction

It has long been known that the Stokes drift in irrotational water waves in otherwise quiescent surroundings transitions from an exponential decay with depth in deep-water waves (Stokes 1847) to quadratic decay in shallow-water waves (Longuet-Higgins 1953). However, that need not be the case when the waves travel on a shear layer of sufficient strength (Phillips & Wu 1994; Phillips & Shen 1996; Phillips 2001*b*; Phillips, Dai & Tjan 2010). Indeed in such circumstances the drift profile can vary dramatically from those above, particularly in shallow-water waves. For that reason Phillips *et al.* (2010) use the broader term 'drift' to describe the averaged nonlinear wave–wave and wave–mean flow interactions arising in such circumstances and reserve the term 'Stokes drift' solely for irrotational waves in otherwise quiescent surroundings.

To be precise they consider two-dimensional monochromatic straight-crested waves of phase velocity $\mathscr{C}$ on, and aligned with, a unidirectional mean shear flow of characteristic velocity $\mathscr{U}$ along the x direction, with z vertical (positive upwards) and y cross-stream. They denote the wave number of the waves by $\mathfrak{K}$ and their wave amplitude by $\mathfrak{a}$ such that their wave slope $\epsilon = \mathfrak{K}\mathfrak{a}$; accordingly, since the characteristic depth of the shear layer is important they define it through the layer depth $\mathfrak{h}$ and let $\alpha = \mathfrak{K}\mathfrak{h}$. Then, since orbital velocities in the wave field are characterized by $\epsilon\mathscr{C}$, it follows that the ratio $\mathscr{U}/\mathscr{C} = O(\epsilon^s)$, where $s \geqslant 0$ and show, finally, that the drift is noticeably different to the Stokes drift whenever $\epsilon^s\alpha^{-2} = O(1)$.

To arrive at this conclusion they restrict attention to small-amplitude waves in which the drift $\boldsymbol{d}$ takes the form (Andrews & McIntyre 1978, see § 2)

$$d_i = \overline{\xi_j \breve{u}_{i,j}} + \tfrac{1}{2}\overline{\xi_j \xi_k}\,\bar{u}_{i,jk} + O(\epsilon^3), \tag{1.1}$$

(here, indices (1, 2, 3) $\mapsto$ (x, y, z) with unit vectors ($\boldsymbol{i}$, $\boldsymbol{j}$, $\boldsymbol{k}$), repeated indices imply summation and commas denote partial differentiation) where $\bar{\boldsymbol{u}}$ is the mean Eulerian velocity, $\breve{\boldsymbol{u}}$ is the Eulerian fluctuating velocity and $\boldsymbol{\xi}$ is the associated particle displacement field. To highlight the importance of each term in (1.1), Phillips *et al.* (2010) note that while the first term would typically be normalized in terms of the wave properties $\mathscr{C}$ and $\mathfrak{K}$, the mean velocity and coordinates in the second term are more appropriately scaled in terms of $\mathscr{U}$ and $\mathfrak{h}$. Then, because the shear flow is unidirectional (Phillips 1998),

$$\bar{\boldsymbol{u}} = \epsilon^s[U(z, t), 0, 0], \tag{1.2}$$

and it transpires that $\epsilon^s\alpha^{-2} = O(1)$ whenever the second term is of the order of the first. On rewriting this expression they further find that

$$\frac{\mathfrak{a}}{\mathfrak{h}} = O\left(\epsilon^{(2-s)/2}\right), \tag{1.3}$$

and conclude that because the physical requirement $\mathfrak{a}/\mathfrak{h} \ll 1$ is satisfied only when $s = 0$ or $s = 1$, the second term in (1.1) must be retained whenever $s \in [0, 1]$.

Of course in the absence of shear or weak shear ($s \geqslant 2$), (1.1) must necessarily recover the Stokes drift, which we now see as a particular limit described by the then only remaining term, the first one. That said, the first term too is affected by shear through $\boldsymbol{\xi}$ (see (4.2) in Phillips *et al.* 2010) and thus should not be interpreted as a general expression for Stokes drift, although such an expression is realizable if the first term is parsed into shear-independent and shear-dependent parts. The key point,

Downloaded from https://www.cambridge.org/core. IFREMER - Brest, on 15 Jan 2017 at 17:03:33, subject to the Cambridge Core terms of use, available at https://www.cambridge.org/core/terms. https://doi.org/10.1017/jfm.2014.37

however, is that the drift is necessarily different from the Stokes drift whenever the second term plays a role. Because of this, Andrews & McIntyre (1978) and Phillips (2001*b*) refer to $\boldsymbol{d}$ as the generalized Stokes drift, although following Phillips *et al.* (2010) we refer to it simply as drift, because physically that is what it is.

We might then ask what s means physically and to answer that we introduce the wave frequency ω. Then $\mathscr{U}/\mathscr{C}$ can be expressed as $\alpha(\mathscr{U}/\mathfrak{h})/\omega$, which is shear/frequency. In the work to follow, however, s rather than ω acts to specify the order of $\mathscr{U}/\mathscr{C}$ and in turn distinguish one class of instability (to Langmuir circulation (LC)) from another (see § 2.3.3). Because of that, Craik (1982) refers to $\mathscr{U}/\mathscr{C}$ simply as the 'shear', using the terms 'strong', 'moderate' and 'weak' shear to concur with the indices $s = 0, 1, 2$. In turn Phillips (1998, 2003) denotes s as the shear index. In the context of wind-driven surface waves then, strong shear indicates that the ratio of the surface velocity to the wave phase velocity is $O(1)$, as is the case with wind-driven surface waves in the laboratory (Veron & Melville 2001). In contrast, s may vary from 0 to 2 in oceanic waters (Melville, Shear & Veron 1998) so there it is customary to introduce a typical level of shear determined by the phase speed of the dominant waves, yielding $s = 2$ or weak (Craik & Leibovich 1976), while in coastal waters with strong tidal currents and/or wind-induced mean flows $s = 1$ or moderate (Marmorino, Smith & Lindemann 2005).

It is this latter ($s \sim 1$) case that Phillips *et al.* (2010) were particularly interested in. Here, with $\epsilon = 0.1$, the requirement $\epsilon^s \alpha^{-2} = O(1)$ is satisfied for $s = 1$ when 1.5 m $< \mathfrak{h} <$ 15 m or, with $s = 1/2$, when 3 m $< \mathfrak{h} <$ 30 m; depths which translate to the shallower end of the inner coastal region. This setting includes, at the deeper end, observations by Gargett *et al.* (2004) (off the New Jersey coast) in which the water is 15 m in depth and the wavelength of the dominant waves is around 100 m, to much shallower water, 2 m in depth, as in the observations of Marmorino *et al.* (2005) (in the Egmont Channel at the mouth of Tampa Bay), where the wavelength of the dominant waves was around 5 m.

Now drift and shear are key ingredients to an instability for the formation of LC and we might wonder whether details of their inception are in turn noticeably affected by detailed changes in the drift? To wit, are shallow-water (in the sense of shallow-water waves) LC different at inception from their deep-water wave counterparts? The object of the present work is to find out.

LC are wind-aligned rolls near the ocean surface that can grow in cross-section to the size of sports stadiums and are crucial to the formation and maintenance of the mixed layer in the upper ocean (Langmuir 1938; Craik & Leibovich 1976; Phillips 2002; Babanin, Ganopolski & Phillips 2009). In contrast, in coastal waters, LC are known to penetrate to the ocean floor and in doing so to enhance vastly the level of sediment mixing (Gargett *et al.* 2004). Typically arising beneath surface waves tens of minutes after the onset of winds above 3 m s^{-1}, LC grow to spacings of several hundred metres (Plueddemann *et al.* 1996), possibly kilometres (Thorpe 2004), and extend windward up to 50 times their spacing (Marmorino *et al.* 2005). Froth-marked rows known as windrows along lines of surface convergence in deep water or suspended particles from the bottom along lines of bottom convergence in shallow water (Hunter & Hill 1980) act to render LC visible, as do dark lines in the infrared owing to a slightly different surface temperature on convergence lines (McLeish 1968; Marmorino, Smith & Lindemann 2004).

Field measurements further highlight a hierarchy of cross-wind scales, of which the largest, and thus the windrow spacing (for a cell pair), is typically two to three times the depth (Smith, Pinkel & Weller 1987; Smith 1992). This is so both in surface layers

Downloaded from https://www.cambridge.org/core. IFREMER - Brest, on 15 Jan 2017 at 17:03:33, subject to the Cambridge Core terms of use, available at https://www.cambridge.org/core/terms. https://doi.org/10.1017/jfm.2014.37

bounded by a thermocline and when the LC extend to the bottom. But documented exceptions arise in the latter case where both visual (Hunter & Hill 1980) and infrared data (Marmorino *et al.* 2005) depict windrow spacings around 10 times the depth. Just how to reconcile this discrepancy is unclear, but doing so is important both as an aid to interpret the surface expressions of LC and to understand the conditions under which LC penetrate to the bottom (Marmorino *et al.* 2005).

Curiously, while there are extensive theoretical studies of LC in deep water, both with and without a surface layer (see, e.g., the review articles by Leibovich 1983; Thorpe 2004, and references therein), there is a dearth (Phillips 2005; Tejada-Martinez & Grosch 2007; Martinat *et al.* 2011) of theoretical work where the water is shallow enough for LC to reach the bottom. Moreover all are based upon the Stokes drift rather than drift.

Key to our study is the credible estimation of LC spacing; an estimation that defers to both the instability mechanism giving rise to LC and the applied boundary conditions. Here we assume the mechanism (see § 2) is CL2 (Craik & Leibovich 1976). CL2 is an inviscid instability mechanism which occurs when the shear is sufficiently weak ($s \geqslant 1$) and of the same sense as the differential drift, at least when the waves are neutral (Phillips 2002, 2003). Various boundary conditions are admissible in CL2 theory, but physical arguments, at least in the large, weigh towards constant stress conditions. That said, while constant stress conditions do act to realize finite onset spacings in deep water (Craik 1977), they appear to shed no light on the preferred spacing in layers above a thermocline where, at least on linear grounds, modes of infinite wavelength are the first to be destabilized.

This conundrum was first addressed by Cox & Leibovich (1993) who note that similar findings occur in thermal convection with thermally insulating boundaries (Sparrow, Goldstein & Jonsson 1964; Nield 1967). They further note that weakly nonlinear effects appear to provide no remedy, because initial perturbations of finite wavelength are found numerically to cascade to larger and larger scales (Chapman & Proctor 1980). In contrast, theoretical considerations show that cells of finite aspect ratio are realized in strongly supercritical nonlinear conditions, even for constant stress boundary conditions (Chapman, Childress & Proctor 1980; Moroz & Leibovich 1985). In seeking an explanation, Cox & Leibovich (1993) point out that constant stress (i.e. Neumann) conditions do not reflect coupling between the perturbed motion and the extra stress it must produce, and argue that coupling, albeit small, occurs (yielding Cauchy boundary conditions). Then by limiting their study to long waves in layers bounded by a strong thermocline they were able to make progress analytically to find on linear stability grounds that the least stable onset spacing is finite. Subsequent studies by Chini & Leibovich (2003, 2005), who consider a weaker thermocline, concur.

But physical arguments lead only so far; the appropriate path is to derive the boundary conditions formally and that we do in § 3.2. We find that the boundary conditions are indeed Cauchy, albeit in a form somewhat richer than Cox & Leibovich (1993) foresaw in which the streamwise and cross-stream wavenumbers play a role, along with gravity and wave frequency. Our plan then is to begin where Cox & Leibovich (1993) left off and relax their restrictions of long waves and uniform shear.

We begin by noting that because the base flow, waves, drift, LC and boundary conditions are interconnected we must pare each from a consistently formulated initial value problem. This we do in § 2. In parsing the problem we observe that three time scales play a role: the wave period, that of the evolving base flow and that of the

Downloaded from https://www.cambridge.org/core. IFREMER - Brest, on 15 Jan 2017 at 17:03:33, subject to the Cambridge Core terms of use, available at https://www.cambridge.org/core/terms. https://doi.org/10.1017/jfm.2014.37

evolving LC. We next note that the latter two scales are long with respect to the wave period and are best averaged over it. But details of the wave field are lost in that average; only quadratic measures of the wave–wave interactions, such as the drift, remain. This means that the wave field and how it is affected by the mean flow must be described separately, which necessitates the concurrent use of both the Navier–Stokes (NS) equation and an averaged form of it, albeit a form that preserves the conservative properties in the mean of NS. Ensuring this property when the wave field is rotational, however, is non-trivial and for that reason we employ the generalized Lagrangian mean (GLM) equations of Andrews & McIntyre (1978) which by design satisfy this requirement. Along the way we find that the GLM equations contract to the mean field CLg equations of Phillips (1998) which describe the base flow and LC for $s \in [0, 2]$ and see that for $s = 1$ they take the same form as the familiar CL equations of Craik & Leibovich (1976), albeit with different scalings for perturbation velocity and time. Specifically for $s = 1$ the cross-stream velocities describing the LC are $O(\epsilon^{3/2})$ while the axial velocity perturbation is $O(\epsilon)$, which are significantly more intense than in the weak shear $s = 2$ deep-water case where velocity perturbations are all $O(\epsilon^2)$. Accordingly the LC grow as $O(\epsilon^{3/2})$ in $s = 1$ shear compared with $O(\epsilon^2)$ in $s = 2$ shear.

We derive the wave field in § 3 along with the aforementioned free-surface boundary conditions. In § 4 we assemble this information into the specific initial value problem for the case at hand along with details of the base flow and drift given previously for the $s = 1$ case by Phillips *et al.* (2010). Results are given in §§ 5 and 6. In § 5 results are given for the simple case of uniform shear and differential drift where we find that Neumann conditions can in fact give rise both to finite preferred cell spacing and also to multiple layers of LC, a feature not reported previously, to the best of the authors' knowledge. In § 6 we allow for more realistic distributions of shear and drift and again observe multiple layers of LC. We discuss our results in § 7.

2. The CLg equations

We consider the formation of LC owing to an instability resulting from the nonlinear interaction of surface gravity waves of characteristic slope $\epsilon \ll 1$ interacting with an evolving sheared mean flow in water of depth $\mathfrak{h}$. The waves give rise to an $O(\epsilon^2)$ drift and, if a viscous boundary condition is present, an $O(\epsilon^2)$ wave induced mean flow. Longuet-Higgins (1953) first investigated $O(\epsilon^2)$ wave induced flows and there are more recent studies by others (e.g. Blondeaux, Brocchini & Vittori 2002; Weber & Ghaffari 2009), but different here is that the mean flow is externally driven and is much stronger, *i.e.* $O(\epsilon)$ compared with its $O(\epsilon^2)$ wave-induced counterpart. Because of that; because the base flow, waves and drift are interconnected; and because we must ensure the initial value problem describing the interaction of each is well posed, we craft the problem from the beginning, taking particular care with the ordering of each part. In fact, the development we outline evolved over a series of earlier papers (Craik 1982; Phillips 1998, 2003; Phillips *et al.* 2010); nevertheless for completeness we give an overview of the relevant points in each and compliment them with a derivation of a consistent set of free-surface boundary conditions.

We begin by noting that three time scales enter the problem, the first being the wave period. On a scale long compared with the wave period is the second, that of an externally driven evolving mean flow. Long too with respect to the wave period

Downloaded from https://www.cambridge.org/core. IFREMER - Brest, on 15 Jan 2017 at 17:03:33, subject to the Cambridge Core terms of use, available at https://www.cambridge.org/core/terms. https://doi.org/10.1017/jfm.2014.37

is the third, that of the evolving LC. We shall quantify each scale later, but for now note that because the time scales of the wave and mean flow are disparate the ensuing wave–mean flow interaction is succinctly described by the GLM equations of Andrews & McIntyre (1978).

Of course for the simplest case of $O(\epsilon)$ waves on an $O(\epsilon^2)$ (i.e. $s=2$) mean flow, the GLM equations relax to the CL equations of Craik & Leibovich (1976) (for the evolution of LC in deep water see Leibovich (1980)). But because the mean flow is not in general restricted to $s=2$, Craik (1982) and subsequently Phillips (1998) (see also Phillips & Wu 1994; Phillips & Shen 1996) considered waves interacting with stronger shear, resulting in what Phillips (2003) denotes the mean field CLg equations ('g' for generalized). Of course the CLg equations also necessarily recover the CL equations in the appropriate (i.e. $s=2$) limit. But they are richer in detail, in that they highlight differences in scaling for both the time and velocity scales of the LC. Moreover, as the level of shear increases, they further highlight the importance to the instability of wave modulation caused by the evolving LC (see e.g. Phillips & Wu 1994; Phillips & Shen 1996; Phillips, Wu & Lumley 1996; Phillips 2005).

A further complication when considering cases in which the shear exceeds $O(\epsilon^2)$ is that admissible waves fields are typically rotational. Amongst other things, this means that mean field equations derived from an Eulerian average of NS do not have the same conservative properties as NS (Phillips 2001*b*). However, such properties are by design retained in the GLM formulation. Of course it is still possible to proceed consistently in multiple-scale problems such as that of interest using Eulerian-averaged NS where we must solve NS side by side with the mean field equations, but our preference is to employ GLM.

We begin then with a brief overview of GLM and go on to review the scalings and expansions relevant to our problem along with expressions governing the mean flow. With this knowledge we then turn to NS and focus first on the wave field and thence boundary conditions at the free surface.

2.1. *GLM theory*

Andrews & McIntyre's (1978) GLM theory is an exact and very general Lagrangian-mean description of the back effect of oscillatory disturbances upon the mean state with no restriction on wave amplitude, although we here restrict attention to waves of small amplitude. In constructing GLM theory, we must first define an exact Lagrangian-mean operator $\overline{(\ )}^L$ corresponding to any given Eulerian-mean operator $\overline{(\ )}$. This necessitates defining with equal generality at location $\boldsymbol{x}$ and time t an exact, disturbance-associated particle displacement field $\boldsymbol{\xi}$ which has zero mean when any average is applied. For any scalar or tensor field φ, it is then possible to write

$$\overline{\varphi(\boldsymbol{x},t)}^L=\overline{\varphi^\xi(\boldsymbol{x},t)},\quad \text{where } \varphi^\xi(\boldsymbol{x},t)=\varphi(\boldsymbol{x}+\boldsymbol{\xi},t). \tag{2.1}$$

Further, provided the mapping $\boldsymbol{x}\mapsto\boldsymbol{x}+\boldsymbol{\xi}$ is diffeomorphic and provided $\overline{\boldsymbol{\xi}(\boldsymbol{x},t)}=0$, there is a unique Lagrangian-mean velocity $\overline{\boldsymbol{u}}^L$ related to any given Eulerian mean velocity $\overline{\boldsymbol{u}}(\boldsymbol{x},t)$ by the drift $\boldsymbol{d}$, as $\overline{\boldsymbol{u}}^L=\overline{\boldsymbol{u}}+\boldsymbol{d}$.

In fact two mean quadratic measures of the nonlinear interaction of the fluctuations with themselves and supporting shear flow arise in GLM theory, the drift $\boldsymbol{d}$ and the pseudomomentum $\boldsymbol{p}$, the latter relaxing to the former when the waves are irrotational (Andrews & McIntyre 1978; Phillips 2001*b*).

Downloaded from https://www.cambridge.org/core. IFREMER - Brest, on 15 Jan 2017 at 17:03:33, subject to the Cambridge Core terms of use, available at https://www.cambridge.org/core/terms. https://doi.org/10.1017/jfm.2014.37

2.1.1. *The generalized Lagrangian-mean equations*

GLM theory is compelling because it satisfies (in inviscid flow) a Kelvin-like theorem akin to that satisfied by the Euler equations. This indicates that GLM exhibits, in the mean, the same conservative properties as does Euler, be the waves rotational or irrotational, and thus that the two sets of equations can be solved simultaneously: NS/Euler to determine admissible wave fields and any modulation to them caused by mean motions; and GLM the effect of said wave field on the mean flow (see e.g. Craik 1982; Phillips & Wu 1994; Phillips & Shen 1996; Phillips 1998, 2005).

When written in a form akin to NS, the GLM momentum equations for homentropic flows of constant density ρ in a non-rotating reference frame, become

$$\bar{q}_{i,t} + \bar{q}_j \bar{q}_{i,j} - p_j(\bar{q}_{j,i} - \bar{q}_{i,j}) + \Pi_i = \mathcal{X}_i, \tag{2.2}$$

where $\bar{\boldsymbol{q}} = \bar{\boldsymbol{u}}^L - \boldsymbol{p}$, and $\boldsymbol{\mathcal{X}}$ allows for dissipative forces, which are discussed in detail by Phillips (1998). Observe that the force term in (2.2) is expressed as $\boldsymbol{p} \times \boldsymbol{\nabla} \times \bar{\boldsymbol{q}}$, that is the cross-product of the pseudomomentum and the vorticity-associated vector field $\mho = \boldsymbol{\nabla} \times \bar{\boldsymbol{q}}$, and contracts to the familiar $\boldsymbol{d} \times \boldsymbol{\nabla} \times \bar{\boldsymbol{u}}$ (sometimes denoted the vortex force) when the waves are irrotational. Further, Π_i includes any external body force F_i (but not the Coriolis force) and $\wp_{,i}$ the gradient of the pressure, force potential (if any) and Bernoulli head, which vanish when we take the curl of (2.2) to realize $\mho$, namely (Phillips 1998)

$$\mho_{i,t} + (\bar{q}_j + \bar{p}_j)\mho_{i,j} = \mho_j(\bar{q}_i + \bar{p}_i)_{,j} - \mho_i(\bar{q}_j + \bar{p}_j)_{,j} + \varepsilon_{ijk}(\mathcal{X}_{k,j} - F_{k,j}) \tag{2.3}$$

where ε_{ijk} is the alternating tensor.

2.2. *Imposed shear of specified strength and $O(\epsilon)$ waves*

Phillips (1998) employs (2.2) and (2.3) to investigate a class of unidirectional shear flows that are subject to a field of small-amplitude waves. He assumes $\mathfrak{h}$ is the characteristic thickness of the shear layer and in the first instance makes variables dimensionless with respect to $\mathfrak{h}$ and $\mathscr{C}$. Then in the event kinematic viscosity ν plays a role, the Reynolds number $\mathfrak{R} \equiv \mathfrak{h}\mathscr{C}/\nu$.

More specifically, for the moment referring to Eulerian variables to fix ideas, he assumes that the flow field $\boldsymbol{u}(x, y, z, t)$ comprises a streamwise-averaged mean portion $\bar{\boldsymbol{u}}(y, z, t)$ in the presence of a wave field $\breve{\boldsymbol{u}}(x, z, t)$, such that $\boldsymbol{u} = \bar{\boldsymbol{u}} + \breve{\boldsymbol{u}}$, where $\boldsymbol{u}$ is necessarily a solution to the NS equations, subject to appropriate boundary conditions. Here the streamwise average is typically over one wavelength, denoted by an overbar on the unscaled variable. The presumption is that the mean flow can be further decomposed into a spanwise (y)-independent portion, which for clarity is depicted by uppercase letters and denoted as the primary flow, and a secondary perturbation flow $\tilde{\boldsymbol{u}}$, such that $\bar{\boldsymbol{u}} = \bar{\boldsymbol{U}} + \tilde{\boldsymbol{u}}$. The task then is to scale each variable and he begins by noting that the mean velocity components better scale with the surface velocity scale $\mathscr{U}$ rather than $\mathscr{C}$ and goes on to introduce a parameter Δ to measure the strength of spanwise-varying perturbations relative to the primary shear flow. No restriction is placed upon the relative time scales of the evolving mean flow and wave field, but for definiteness the mindset is that they are disparate with the mean flow having the longer time scale. Then, if the wave field is $O(\epsilon)$

$$\boldsymbol{u} = \bar{\boldsymbol{U}} + \tilde{\boldsymbol{u}} + \breve{\boldsymbol{u}} = \epsilon^s\{\boldsymbol{U}(z, t) + \Delta \boldsymbol{u}(y, z, t)\} + \epsilon \breve{\boldsymbol{U}}(x, z, t) + O(\epsilon^{s+1}\Delta). \tag{2.4}$$

Downloaded from https://www.cambridge.org/core. IFREMER - Brest, on 15 Jan 2017 at 17:03:33, subject to the Cambridge Core terms of use, available at https://www.cambridge.org/core/terms. https://doi.org/10.1017/jfm.2014.37

In less familiar GLM variables, the velocity-associated mean vector field $\bar{\boldsymbol{q}}(y, z, t)$ concordant to $\bar{\boldsymbol{u}}$ is then

$$\bar{\boldsymbol{q}} = \bar{\boldsymbol{Q}} + \tilde{\boldsymbol{q}} = \epsilon^s\{[Q_1, 0, \epsilon^{2-s}Q_3] + \Delta[q_1, \epsilon^n q_2, \epsilon^n q_3]\} + O(\epsilon^{s+1}\Delta) \quad (n \geqslant 0). \tag{2.5}$$

Note that the power n, which is included for generality, can have values other than zero and that n is related to s, as we shall shortly see. Note too that although $\breve{\boldsymbol{u}}$ vanishes in a streamwise average, the influence of the wave field is evident in the Lagrangian mean as fields of pseudomomentum and drift which, as indicated above, act to relate the Eulerian and Lagrangian mean velocity fields through $\bar{\boldsymbol{q}} = \bar{\boldsymbol{u}} + \boldsymbol{d} - \boldsymbol{p}$. Of course to lead order the averaged quadratic measures $\boldsymbol{d}$ and $\boldsymbol{p}$ are $O(\epsilon^2)$. But, because evolving velocity perturbations may in turn modulate the wave field, that modulation will produce spanwise-varying components of drift and pseudomomentum (Craik 1982; Phillips 1998). As a consequence $\boldsymbol{p}$ is expanded as

$$\boldsymbol{p}(y, z, t) = \epsilon^2\{[P_1, 0, P_3] + \epsilon^s\Delta[p_1, \epsilon^n p_2, \epsilon^n p_3 + \cdots]\} \tag{2.6}$$

and similarly for $\boldsymbol{d}$, along with the affiliated field

$$\Pi_i = F_i + \wp_{,i} = F_i + \epsilon^s[\mathcal{G}_{,i}(x, z, t) + \Delta g_{,i}(y, z, t) + \cdots]. \tag{2.7}$$

2.3. *The CLg equations*

2.3.1. *Conservation of mass*

GLM flows are typically not divergence free as we see from mass conservation, which requires

$$\bar{D}^L J + J(q_i + p_i)_{,i} = 0, \tag{2.8}$$

where J is the Jacobian of the mapping $\boldsymbol{x} \mapsto \boldsymbol{x} + \boldsymbol{\xi}$. Nevertheless, because $\bar{u}_{i,i} = (\bar{q}_i + p_i - d_i)_{,i} = 0$, we see for example that $q_2 = u_2 + \epsilon^2(d_2 - p_2)$ and are thus at liberty to introduce the perturbation stream function ψ as

$$q_2 = \frac{\partial\psi}{\partial z} \quad \text{and} \quad q_3 = -\frac{\partial\psi}{\partial y}. \tag{2.9}$$

2.3.2. *The primary flow field*

The primary flow field follows by substituting (2.5) and (2.6) into (2.2). Then, because (2.5) must identically satisfy (2.2) with $q_1, q_2, q_3 = 0$ and because Π here reduces to the mean streamwise body force G, the x-momentum equation takes the form (Phillips 1998)

$$\frac{\partial Q_1}{\partial\tau} + \epsilon^2\mathfrak{R}D_3\frac{\partial Q_1}{\partial z} = -G + \frac{\partial^2}{\partial z^2}\left(Q_1 - \epsilon^{2-s}(D_1 - P_1)\right), \tag{2.10}$$

where time has been rescaled as $\tau = \mathfrak{R}^{-1}t$ and $G = \mathfrak{R}\partial\mathcal{G}/\partial x$.

It is important to note here that because $Q_1 = U + \epsilon^{2-s}(D_1 - P_1)$, the primary flow Q_1 is dominated by its Eulerian counterpart U for all $s \leqslant 1$. This is not to say the wave field is impotent; on the contrary, it induces (in the presence of viscous boundary) an associated Eulerian flow of the same order as the $O(\epsilon^2)$ rectified wave field, as Longuet-Higgins (1953) long ago determined. But for $s = 1$ that $O(\epsilon^2)$ induced flow appears solely as a higher-order correction to the $O(\epsilon)$ primary flow U and thus here plays no significant role.

Downloaded from https://www.cambridge.org/core. IFREMER - Brest, on 15 Jan 2017 at 17:03:33, subject to the Cambridge Core terms of use, available at https://www.cambridge.org/core/terms. https://doi.org/10.1017/jfm.2014.37

2.3.3. *The secondary flow field*

To determine the secondary flow we again substitute (2.5) and (2.6) into (2.2), but this time subtract (2.10), which leads to the $O(\epsilon^s\Delta)$ streamwise evolution equation for q_1, while the same expansions and (2.3) yield the $O(\epsilon^{s+n}\Delta)$ streamwise component of the vorticity-associated vector field. For this general form we refer the reader to § 4 in Phillips (1998). Rather here, since our interest is with structure arising through an instability requiring $\partial P_1/\partial z \neq 0$, we restrict attention to that case for which time is rescaled as $\mathfrak{t} = \epsilon^{(s+2)/2}(t - t_0)$, with t_0 being an arbitrary time at which the secondary flow initiates, and $n = (2 - s)/2$. Then on assuming a body force $\boldsymbol{k}\cdot\boldsymbol{F} = \mathfrak{h}\mathscr{C}\mathfrak{S}\Delta\vartheta$, where details of $\mathfrak{S}$ ensure dimensional consistency and ϑ is defined in § 2.4, we find (Phillips 1998)

$$\frac{\partial q_1}{\partial \mathfrak{t}} + \Delta\left(q_2\frac{\partial q_1}{\partial y} + q_3\frac{\partial q_1}{\partial z}\right) + \epsilon^{(2-s)/2}D_3\frac{\partial q_1}{\partial z} + q_3\frac{\partial Q_1}{\partial z} = \epsilon^{-(s+2)/2}\mathfrak{R}^{-1}\nabla^2 q_1 + O\left(\epsilon^{(2-s)/2}\mathfrak{R}^{-1}\right) \tag{2.11}$$

and

$$\begin{aligned}\frac{\partial \mathcal{U}_1}{\partial \mathfrak{t}} + \Delta\left(\frac{\partial \mathcal{U}_1 q_2}{\partial y} + \frac{\partial \mathcal{U}_1 q_3}{\partial z}\right) + \epsilon^{(2-s)/2}\frac{\partial}{\partial z}(\mathcal{U}_1 D_3) + \frac{\partial q_1}{\partial y}\frac{\partial P_1}{\partial z} \\ - \epsilon^s\frac{\partial Q_1}{\partial z}\frac{\partial p_1}{\partial y} + \epsilon^s\Delta\left(\frac{\partial q_1}{\partial y}\frac{\partial p_1}{\partial z} - \frac{\partial q_1}{\partial z}\frac{\partial p_1}{\partial y}\right) \\ = \epsilon^{-(s+2)/2}\mathfrak{R}^{-1}\nabla^2\mathcal{U}_1 - \epsilon^{-(s+2)}\mathfrak{S}\frac{\partial \vartheta}{\partial y} + O\left(\epsilon^{(2-s)/2}\mathfrak{R}^{-1}\right).\end{aligned} \tag{2.12}$$

Note that because n varies with s it is evident from (2.5) that transverse and axial velocity perturbations may differ in order, a point first made by Craik (1982). Furthermore, although the evolving secondary flow distorts the wave field (see § 3.2) giving rise to p_1, the term containing p_1 in (2.12) is premultiplied by ϵ^s, suggesting that wave modulation affects the mean field significantly only in the $s = 0$ case (see e.g. Phillips & Wu 1994; Phillips & Shen 1996). However we will not from this point exclude wave modulation. This may appear odd to readers new to multiscale problems, but the point is that effects which appear unimportant part way through the analysis cannot be fully assessed until the analysis is complete. Indeed we shall find (in § 3.2) that the boundary conditions on the mean flow are affected by wave modulation, even when $s = 1$. That notwithstanding, wave distortion in the y and z directions is $O(\epsilon^{3+s/2}\Delta)$ and may be neglected for all $s \in [0, 2]$, allowing us to rewrite (2.9) as

$$\frac{\partial q_2}{\partial y} + \frac{\partial q_3}{\partial z} = 0 \quad \text{and thus} \quad \mathcal{U}_1 = -\nabla^2\psi. \tag{2.13}$$

2.4. *The energy equation*

The CLg equations are rendered complete by an energy equation which accounts for rotational waves in all levels of shear. Since thermal effects were not considered by Phillips (1998) and the CL energy equation (Leibovich 1977) is restricted to irrotational waves and weak shear, Phillips (2002) derives a more general expression. In accord with the CL formulation, however, he employs the Boussinesq approximation, replaces density by temperature and writes the streamwise-averaged dimensionless temperature as

$$\bar{\theta}(\boldsymbol{x}, t) = \Theta(z) + \theta(\boldsymbol{x}, t) \tag{2.14}$$

Downloaded from https://www.cambridge.org/core. IFREMER - Brest, on 15 Jan 2017 at 17:03:33, subject to the Cambridge Core terms of use, available at https://www.cambridge.org/core/terms. https://doi.org/10.1017/jfm.2014.37

where $\bar{\theta}(\boldsymbol{x}, t_0) = \Theta(z)$ and $\theta(\boldsymbol{x}, t_0) = 0$ at some initial time $t = t_0$. With the usual approximations of thermal convection, the temperature is then governed by the energy equation which is, in GLM form,

$$\frac{\partial \theta}{\partial t} + \bar{\boldsymbol{q}} \cdot \nabla \theta = -\boldsymbol{k} \cdot (\bar{\boldsymbol{q}} + \boldsymbol{p}) \frac{\mathrm{d}\Theta}{\mathrm{d}z} + \kappa^* \nabla^2 \theta, \tag{2.15}$$

where the thermal diffusivity is $\kappa = \kappa^* \mathfrak{h}\mathscr{C}$.

As above, our intent is to isolate spanwise-independent primary fields and spanwise-dependent secondary fields. More specifically we are interested in the modification of the primary temperature field due to the wave field through D_3. So on setting

$$\theta = \epsilon^2 \Theta(z, t) + \Delta \vartheta(y, z, t), \tag{2.16}$$

it follows that the wave-induced evolution of the primary temperature field is described by Phillips (2002)

$$\frac{\partial \Theta}{\partial t} + \epsilon^2 Q_3 \frac{\partial \Theta}{\partial z} = -D_3 \frac{\mathrm{d}\Theta}{\mathrm{d}z} + \kappa^* \frac{\partial^2 \Theta}{\partial z^2} \tag{2.17}$$

while the evolution equation for the secondary temperature field becomes (Phillips 2002)

$$\frac{\partial \vartheta}{\partial \mathfrak{t}} + \Delta \boldsymbol{q} \cdot \nabla \vartheta = -(q_3 + \epsilon^2 p_3) \frac{\mathrm{d}\Theta}{\mathrm{d}z} - \epsilon^2 q_3 \frac{\partial \Theta}{\partial z} - \epsilon^{(2-s)/2} Q_3 \frac{\partial \vartheta}{\partial z} + \epsilon^{-(s+2)/2} \kappa^* \nabla^2 \vartheta, \tag{2.18}$$

where $\boldsymbol{q} = [q_2, q_3]$.

2.5. *The case* $s = 1$

In the $s = 2$ limit, of course, the CLg equations reduce to the CL equations of Craik & Leibovich (1976), in which the time scale of any evolving structure is $\mathfrak{t} = \epsilon^2 t$, while velocity scales as $\bar{\boldsymbol{q}} = (\epsilon^2(U + u), \epsilon^2 v, \epsilon^2 w)$. (Note that because the wavefield is here irrotational, then $P_1 = D_1$ so that $\bar{\boldsymbol{q}} = \bar{\boldsymbol{u}}$.) When $s = 1$, on the other hand, the time scale is $\mathfrak{t} = \epsilon^{3/2} t$ and because $n = 1/2$, we see that $\bar{\boldsymbol{q}} = (\epsilon(U + u), \epsilon^{3/2} v, \epsilon^{3/2} w)$. In § 4 we shall further find that $P_1 = D_1 + O(\epsilon)$ (Phillips *et al.* 2010) which means that $Q_1 = U + O(\epsilon)$ so that the linearized CLg equations here too have the same form as the CL equations, albeit with scaling appropriate to $s = 1$, namely

$$\frac{\partial U}{\partial \tau} - \frac{\partial^2 U}{\partial z^2} = -G \tag{2.19a}$$

with

$$\frac{\partial u}{\partial \mathfrak{t}} - \epsilon^{-3/2} \mathfrak{R}^{-1} \nabla^2 u = -w \frac{\partial U}{\partial z}, \tag{2.19b}$$

$$\frac{\partial \mho_1}{\partial \mathfrak{t}} - \epsilon^{-3/2} \mathfrak{R}^{-1} \nabla^2 \mho_1 = -\frac{\partial u}{\partial y} \frac{\partial D_1}{\partial z} - \epsilon^{-3} \mathfrak{S} \frac{\partial \vartheta}{\partial y} \tag{2.19c}$$

and

$$\frac{\partial \vartheta}{\partial \mathfrak{t}} - \epsilon^{-3/2} \kappa^* \nabla^2 \vartheta = -w \frac{\mathrm{d}\Theta}{\mathrm{d}z}. \tag{2.19d}$$

We will return to the equation set (2.19) in § 4 and focus now on the wave fields whose time scale is smaller than that of the evolving secondary field and must be determined from NS.

Downloaded from https://www.cambridge.org/core. IFREMER - Brest, on 15 Jan 2017 at 17:03:33, subject to the Cambridge Core terms of use, available at https://www.cambridge.org/core/terms. https://doi.org/10.1017/jfm.2014.37

3. Wave field and boundary conditions

To recap in Eulerian variables, we have an initial value problem for $\boldsymbol{u}$ which, in (2.4), we parsed into three parts $\bar{\boldsymbol{u}} + \tilde{\boldsymbol{u}} + \breve{\boldsymbol{u}}$ each with its own time scale. The first two involve a streamwise average and are specified by (2.19). But although $\breve{\boldsymbol{u}}$ vanishes in that average, averaged nonlinear interactions resulting from it remain as D_1 and to determine D_1 we require the wave field $\breve{\boldsymbol{u}}$. This we find from NS. In fact Phillips *et al.* (2010) have previously deduced $\breve{\boldsymbol{u}}$ and D_1 for the $s = 1$ case and so we shall give no more than a brief outline of that derivation (in § 3.1). Not previously derived, however, is a consistent set of free-surface boundary conditions for $\boldsymbol{u}$ which are necessary to render the initial value problem for $s = 1$ well posed. These too are found from NS using a method introduced by Phillips (2005) for free-surface waves on ($s = 0$) shear.

Consider then a layer of liquid in which we identify $z = 0$ with the mean free surface and $z = -1$ with its base, which for now we consider rigid, but it need not be. Of interest are admissible wave fields $\breve{\boldsymbol{u}}$ in the presence of the mean flow $\bar{\boldsymbol{U}} + \tilde{\boldsymbol{u}}$, which together total $\boldsymbol{u}$ as (defined in (2.4)) and satisfy NS.

3.1. *Wave equations*

To fix ideas we restrict ourselves to monochromatic two-dimensional waves which we decompose into $O(\epsilon)$ and $O(\epsilon^{s+1})$ components that each satisfy continuity,

$$\breve{\boldsymbol{u}}(x, y, z, t) = \epsilon[\Phi', 0, -\mathrm{i}\alpha\Phi]\mathrm{e}^{\mathrm{i}\beta} + \epsilon^{s+1}[\phi', 0, -\mathrm{i}\alpha\phi]\mathrm{e}^{\mathrm{i}\beta} + \breve{\boldsymbol{u}}^*, \tag{3.1}$$

but which at higher order may be subject to spanwise distortion through $\breve{\boldsymbol{u}}^*(x, y, z, t)$. Here Φ and ϕ are functions only of z and prime denotes $\mathrm{d}/\mathrm{d}z$. Further $\beta = \alpha x - \omega_0 t$ and for generality $\omega_0 = \omega + \epsilon^s\omega_2$, where $\mathscr{C}\omega_0/\mathfrak{h}$ is the wave frequency. On substituting (2.4) into NS (normalized as in § 2 by $\mathscr{C}$ and $\mathfrak{h}$) and then subtracting (2.19*a*) followed by cross-eliminating pressure and collecting the fundamental mode $\mathrm{e}^{\mathrm{i}\beta}$ at successive orders, we find variants of the Orr–Sommerfeld equation. Because our flow field is devoid of critical layers, however, we do not expect viscous eigensolutions to play a significant role, and thus take the inviscid limit, to find for $s = 1$ that

$$\epsilon[\omega\Phi'' - \omega\alpha^2\Phi] + \epsilon^2[\omega\phi'' - \omega\alpha^2\phi + \alpha U''\Phi] = 0. \tag{3.2}$$

From (3.2) then, the governing equations at successive orders are thus a shortened Rayleigh equation subject to boundary conditions (3.10*b*,*c*), depicting $O(\epsilon)$ irrotational waves

$$\Phi'' - \alpha^2\Phi = 0 \tag{3.3}$$

and a further Rayleigh equation subject to boundary conditions (3.11*a*,*b*) at $O(\epsilon^2)$, depicting rotational waves:

$$\phi'' - \alpha^2\phi = -\frac{\alpha}{\omega}U''\Phi. \tag{3.4}$$

Phillips *et al.* (2010) note that only the $O(\epsilon)$ solution is necessary to deduce D_1 for the $s = 1$ case and that the solution to (3.3) is (Longuet-Higgins 1953)

$$\Phi = \frac{\omega}{\alpha^2}\frac{\sinh\alpha(z+1)}{\sinh\alpha} \quad \text{with } \omega = \sqrt{\mathfrak{g}\alpha\tanh\alpha}, \tag{3.5a,b}$$

where $\mathscr{C}^2\mathfrak{g}/\mathfrak{h}$ is gravity.

Downloaded from https://www.cambridge.org/core. IFREMER - Brest, on 15 Jan 2017 at 17:03:33, subject to the Cambridge Core terms of use, available at https://www.cambridge.org/core/terms. https://doi.org/10.1017/jfm.2014.37

3.2. *Free-surface and other boundary conditions*

Equations (2.19), (3.3) and (3.4) each require boundary conditions at the mean free surface and the bottom. Since one equation is averaged and the other not it is tempting to derive the averaged one from GLM and the other from NS. But doing so is unwise, because nonlinearities resulting from the product of two variables harmonic in x can realize an x-independent component that may be overlooked. Instead we follow Phillips (2005) and invoke no average. Here, rather than introduce some sort of stress condition, we instead apply the momentum equation (NS) on the surface and pare the boundary conditions into x-independent and x-dependent parts.

Appropriate boundary conditions are (the kinematic condition) that the free surface be a material surface of the fluid and (the dynamic condition) that there be continuity of pressure $\rho\mathscr{C}^2\mathfrak{p}$ at the surface. But because our wave field may be weakly rotational and because viscous stresses may play a role, we cannot employ the Bernoulli form to derive the dynamic condition. Instead we must require, in the absence of surface tension and with the position of the free surface given by $z=\eta(x, y, t)$, that

$$\frac{\mathrm{D}(z-\eta)}{\mathrm{D}t}=0 \quad \text{and} \quad \frac{\mathrm{D}\boldsymbol{u}}{\mathrm{D}t}=-\nabla\mathfrak{p}+\boldsymbol{k}\mathfrak{g}+\mathfrak{R}^{-1}\nabla^2\boldsymbol{u} \quad \text{on } z=\eta. \tag{3.6a,b}$$

We then note that $\nabla\mathfrak{p}$ has no component lying along the free surface, which means that $\nabla\mathfrak{p}$ is along the vector $\nabla(z-\eta)$; so

$$\nabla\mathfrak{p}=\frac{\partial\mathfrak{p}}{\partial z}\nabla(z-\eta) \quad \text{on } z=\eta. \tag{3.7}$$

Then $\nabla\mathfrak{p}$ on $z=\eta$ may be expressed in terms of variables on $z=0$ using Taylor's theorem.

As in § 2.2 we employ the decomposition (2.4), namely $\boldsymbol{u}(x, y, z, t)=\boldsymbol{U}+\breve{\boldsymbol{u}}+\tilde{\boldsymbol{u}}$ in which $\boldsymbol{U}=\epsilon[U, 0, 0]$ is the imposed mean flow and the wave field is composed of neutral waves $\breve{\boldsymbol{u}}$ as defined in (3.1). Finally, we express $\tilde{\boldsymbol{u}}$ and $\breve{\boldsymbol{u}}^*$ in accord with (2.5) and (3.1) for $s=1$ that (i) assumes spanwise periodicity with wavenumber l and (ii) allows for any $O(\epsilon^2\Delta)$ distortion of the wave field by the perturbation field, namely

$$\tilde{\boldsymbol{u}}(y, z, \mathfrak{t})=\epsilon\Delta\left[\mathfrak{u}(z, \mathfrak{t})\cos ly, \epsilon^{1/2}\mathfrak{v}(z, \mathfrak{t})\sin ly, \epsilon^{1/2}\mathfrak{w}(z, \mathfrak{t})\cos ly\right] \tag{3.8a}$$

and

$$\breve{\boldsymbol{u}}^*=\epsilon^2\Delta[\mathfrak{U}(z, t)\cos ly, \mathfrak{V}(z, t)\sin ly, \mathfrak{W}(z, t)\cos ly]\mathrm{e}^{\mathrm{i}\beta}+O(\epsilon^3\,\Delta). \tag{3.8b}$$

To satisfy continuity we further require that $l\mathfrak{v}+\mathfrak{w}'=0$ and $i\alpha\mathfrak{U}+l\mathfrak{W}+\mathfrak{W}'=0$, where $(\mathfrak{u}, \mathfrak{v}, \mathfrak{w})$ and $(\mathfrak{U}, \mathfrak{V}, \mathfrak{W})$ are appropriate component velocities in (x, y, z).

Now the liquid surface is planar in the undisturbed state (so $\eta=0$), the velocity field is $\boldsymbol{U}$ and the pressure is specified by the hydrostatic law $\mathfrak{p}=-\mathfrak{g}z$. But when small, time-dependent three-dimensional perturbations are present, the free surface moves to $z=\eta$, thereby introducing an excess pressure at all z. In order to determine this pressure and ascertain boundary conditions at each order, we first expand $\mathfrak{p}$ and η in accord with (2.4) and (3.8*b*). Of course the detailed form of each is not known *a priori*, but after carrying out the expansion we are left with

$$\mathfrak{p}=\mathcal{P}_0(z)+\mathrm{e}^{\mathrm{i}\beta}\left\{\epsilon\mathcal{P}_1(z)+\left[\epsilon^2\Delta\mathrm{i}\mathcal{P}_2(z, \mathfrak{t})+\epsilon^{5/2}\Delta\alpha\mathcal{P}_3(z, \mathfrak{t})\right]\cos ly\right\}+O(\epsilon^3\Delta) \tag{3.9a}$$

Downloaded from https://www.cambridge.org/core. IFREMER - Brest, on 15 Jan 2017 at 17:03:33, subject to the Cambridge Core terms of use, available at https://www.cambridge.org/core/terms. https://doi.org/10.1017/jfm.2014.37

and

$$\eta = \eta_0 + \mathrm{e}^{\mathrm{i}\beta}\left\{\epsilon\alpha^{-1}\eta_1 + \epsilon^{3/2}\Delta\left[\mathrm{e}^{-\mathrm{i}\beta}\eta_2(\mathfrak{t}) + \epsilon^{1/2}\eta_3(\mathfrak{t}) + \epsilon\mathrm{i}\eta_4(\mathfrak{t})\right]\cos ly\right\} + O(\epsilon^3\Delta). \quad (3.9b)$$

On substituting (3.1), (3.8*b*) and (3.9*a*) into (3.6) and collecting terms at each order we find at $O(1)$ that $\mathcal{P}_0 = -\mathfrak{g}z$; further, with no loss of generality, we set $\eta_0 = 0$. Accordingly at $O(\epsilon)$ on $z = 0$ we find

$$\eta_1 = 1 \quad \text{with } \alpha^2\Phi = \omega, \quad \omega\Phi' = \mathfrak{g} \quad \text{and} \quad \mathcal{P}_1{}' = \alpha\omega\Phi. \quad (3.10a,b,c)$$

In concert with (3.10) we further have $U' = \zeta$, where ζ is a constant indicative of any external viscous stress acting on $z = 0$ over the time scale $\tau = O(1)$ (see § 4.2). Proceeding now to $O(\epsilon^2)$, we have on $z = 0$ (Phillips *et al.* 2010)

$$\alpha\phi = \frac{\omega_2}{\alpha} - U \quad \text{and} \quad \omega\phi' = \alpha U\Phi' - \omega_2\Phi' - \alpha U'\Phi \quad (3.11a,b)$$

which serve as boundary conditions for (3.4).

In order to find a boundary condition for $\mathfrak{u}$, however, we must proceed to $O(\epsilon^2\Delta)$ where, after some algebra and after elimination of $\mathfrak{U}$, $\mathfrak{V}$ and $\mathfrak{W}$, we find on $z = 0$ that

$$\mathfrak{u}' - \frac{(\alpha^2 + l^2)\Phi'}{\alpha^2\Phi}\mathfrak{u} = 0 \quad \text{with } \mathcal{P}_2{}'' = -\frac{(\alpha^2 + l^2)\Phi'}{\alpha^2\Phi}\mathcal{P}_2{}' \quad \text{and} \quad \eta_3 = \omega^{-2}(2\omega\mathfrak{u} + \mathcal{P}_2{}') \quad (3.12a,b,c)$$

and, correspondingly, proceed to $O(\epsilon^{5/2}\Delta)$ for boundary conditions for $\mathfrak{w}$ and $\mathfrak{v}$, to find

$$\mathfrak{w}' + \frac{\Phi'\mathfrak{w}}{\Phi} = 0 \quad \text{with } \mathfrak{w}'' - l^2\mathfrak{w} = 0 \quad \text{and} \quad \eta_4 = \frac{\omega\mathfrak{w}}{\alpha\mathfrak{g}} \quad \text{on } z = 0. \quad (3.13a,b,c)$$

Now from (3.5) and (3.10) we know on $z = 0$ that $\Phi'/\Phi = \alpha\mathfrak{g}/\omega^2 = \alpha/\tanh(\alpha)$, so we see that our boundary conditions involve gravity, wave frequency and the streamwise and spanwise wavenumbers. Furthermore they contract, as $\alpha \to 0$ and $l \neq 0$ to (since $\Phi'/\Phi \sim 1$) the simple set $\mathfrak{u} = 0$, $\mathfrak{w}' + \mathfrak{w} = 0$ and $\mathfrak{w}'' - l^2\mathfrak{w} = 0$. Alternatively for $\alpha \gg 1$ we note that $\Phi'/\Phi \sim \alpha$ causing the boundary conditions to reduce to $\mathfrak{w}''$, $\mathfrak{w}$, $\mathfrak{u} \sim 0$. In short, we see that provided $\mathfrak{w} \neq 0$, then (3.12*a*) and (3.13*a*) are Cauchy for finite α and l.

But does $\mathfrak{w}$ not vanish on the plane $z = 0$? The answer is yes in an Eulerian mean sense but not necessarily in a Lagrangian mean sense. Why? Because the Lagrangian mean of the value of z at which the free surface occurs, taken over one wavelength (or one wave period), need not be $z = 0$. Accordingly the modulation to the wave amplitude η_4, and thus $\mathfrak{w}$, need not be zero at $z = 0$.

In contrast the mean primary flow, wave field and velocity perturbations must vanish at the rigid bottom $z = -1$, so there we require that $\boldsymbol{U} = 0$, $\breve{\boldsymbol{u}} = 0$ and $\tilde{\boldsymbol{u}} = 0$, from which it follows that

$$U = 0, \quad \mathfrak{u} = 0 \quad \text{with } \mathfrak{w}' = \mathfrak{w} = 0 \quad \text{on } z = -1. \quad (3.14)$$

4. Initial value problem

Our task now is to specialize the preceding formulation into an initial value problem relevant to the formation of LC beneath waves of characteristic slope $\epsilon \ll 1$ that

Downloaded from https://www.cambridge.org/core. IFREMER - Brest, on 15 Jan 2017 at 17:03:33, subject to the Cambridge Core terms of use, available at https://www.cambridge.org/core/terms. https://doi.org/10.1017/jfm.2014.37

propagate with phase velocity $\mathscr{C}$ on a sheared flow whose characteristic velocity is $\mathscr{U}$ such that $\mathscr{U}/\mathscr{C} = O(\epsilon)$ in water of depth $\mathfrak{h}$.

We begin with the water initially at rest and at constant temperature and exclude thermal effects so $\mathfrak{S} = 0$. Then at time $t = 0$ either a wind stress ζ is applied to the $z = 0$ plane or a body force G is imposed throughout the water column. At any interior point in the water, the velocity then increases with time giving rise to a primary flow in what we define as the x direction. A complimentary wave field also propagating in the x direction is imposed at a later time, $t = t_0$ say.

The ensuing $O(\epsilon)$ wave–$O(\epsilon)$ mean flow interaction is described by the CLg equations (2.19) which may be written to contain a parameter that can be expressed as a Langmuir number (Craik & Leibovich 1976) or a Rayleigh number $\mathcal{R}$ (Cox & Leibovich 1993); we choose the latter. To proceed we rewrite (2.19) in terms of $(\mathfrak{u}, \mathfrak{v}, \mathfrak{w})$. Herein time must scale as $\mathfrak{t}\mathfrak{h}^2\nu_T^{-1}$, where ν_T is an eddy viscosity representative of the turbulent diffusivity of momentum. Spatial scales remain $(x, y, z)\mathfrak{h}$. Since the axial component of velocity is $\epsilon\mathscr{C}(U + u) = \mathscr{U}(U + \mathfrak{u})$, we find that the component velocities must scale as

$$[(U(z, t) + \mathfrak{u}(y, z, t))\mathscr{U}, (\mathfrak{v}(y, z, t), \mathfrak{w}(y, z, t))\nu_T/\mathfrak{h}]. \tag{4.1}$$

To fix ideas we think of $\mathscr{U}$ as the mean velocity at the free surface in the limit $\tau \to \infty$. It remains to scale the drift (or pseudomomentum) and here we write $\epsilon^2\mathscr{C}D_1 = \mathscr{D}D$, where $\mathscr{D}$ is a measure of the drift, its maximum say (see § 4.3). We can then introduce $\mathcal{R}$, defined below.

Returning now to (2.19), we see that our equation for the primary flow remains

$$\frac{\partial U}{\partial \tau} - \frac{\partial^2 U}{\partial z^2} = -G, \tag{4.2a}$$

while, on assuming spanwise periodicity with wavenumber l as per (3.8*b*), our evolution equations for the secondary flow become

$$\frac{\partial \mathfrak{u}}{\partial \mathfrak{t}} - (\mathrm{D}^2 - l^2)\mathfrak{u} = -\mathfrak{w}U' \tag{4.2b}$$

and

$$(\mathrm{D}^2 - l^2)\frac{\partial \mathfrak{w}}{\partial \mathfrak{t}} - (\mathrm{D}^2 - l^2)^2\mathfrak{w} = \mathcal{R}l^2\mathfrak{u}D', \tag{4.2c}$$

where

$$\mathcal{R} = \frac{\mathscr{U}\mathscr{D}\mathfrak{h}^2}{\nu_T^2} \quad \text{and} \quad \mathrm{D}^2 = \frac{\mathrm{d}^2}{\mathrm{d}z^2}. \tag{4.3}$$

Note that the primary U and secondary $(\mathfrak{u}, \mathfrak{v}, \mathfrak{w})$ flows evolve on time scales $\tau = \mathfrak{R}^{-1}t$ and $\mathfrak{t} = \epsilon^{3/2}t$, respectively, and are disparate unless $\epsilon^{3/2}\mathfrak{R} = O(1)$, which is unlikely. In fact, typically $\mathfrak{R} \gg \epsilon^{-3/2}$, which means that the primary flow grows over a time scale long with respect to the LC. This disparity allows us to treat τ as a parameter and, since LC initiate at t_0, to specify $\tau > 0$ at $\mathfrak{t} = 0$. To proceed we require U', D' and boundary conditions.

Downloaded from https://www.cambridge.org/core. IFREMER - Brest, on 15 Jan 2017 at 17:03:33, subject to the Cambridge Core terms of use, available at https://www.cambridge.org/core/terms. https://doi.org/10.1017/jfm.2014.37

4.1. *Boundary conditions*

Free-surface and rigid-bottom boundary conditions for the $s=1$ case were derived in § 3.2. Hence, in view of (3.12) and (3.13) we write

$$U'=\zeta, \quad \mathfrak{u}'-\kappa\alpha^*\mathfrak{u}=\mathfrak{w}''+\frac{l^2}{\alpha^*}\mathfrak{w}'=\mathfrak{w}''-l^2\mathfrak{w}=0 \quad \text{on } z=0 \tag{4.4a,b,c,d}$$

and

$$U=0, \quad \mathfrak{u}=\mathfrak{w}'=\mathfrak{w}=0 \quad \text{on } z=-1, \tag{4.5a,b,c,d}$$

where

$$\kappa=\frac{\alpha^2+l^2}{\alpha^2} \quad \text{and} \quad \alpha^*=\frac{\alpha}{\tanh\alpha}. \tag{4.6}$$

4.2. *Base flow*

The CL2 instability is wave driven (McIntyre & Norton 1990; Phillips 2003) and draws energy from the shear U' through the differential drift D'. Consistent profiles for both for $s=1$ flows were derived by Phillips *et al.* (2010) as outlined below.

4.2.1. *Rayleigh stress problem in water of finite depth*

Our first candidate for the base flow is in the Couette class and results from a constant stress $U'(0,\tau)=\zeta=1$ applied at the free surface $z=0$ for $\tau>0$ with a rigid no slip boundary at the base $z=-1$. Then on solving (4.2*a*) subject to (4.4*a*) and (4.5*a*) with $G=0$ the velocity gradient is (Phillips *et al.* 2010)

$$U'(z,\tau)=1-\frac{8}{\pi^2}\sum_{n=0}^{\infty}\frac{\pi}{2(2n+1)}\exp\left[-\left(n+\frac{1}{2}\right)^2\pi^2\tau\right]\sin\left(n+\frac{1}{2}\right)\pi z. \tag{4.7}$$

Observe that $U'(z,\tau)\to 1$ as $\tau\to\infty$ indicating that the solution recovers Couette flow as it must.

4.2.2. *Starting pressure-driven flow*

Our second candidate is in the Poiseuille class and mimics a pressure-driven flow representative of a current with a rigid boundary at $z=-1$ and zero imposed tangential stress at the free surface $z=0$. Here we again solve (4.2*a*) subject to (4.4*a*) and (4.5*a*) albeit with $\zeta=0$ and $G\neq 0$; then (Phillips *et al.* 2010)

$$U'=G\left\{z+\frac{8}{\pi^2}\sum_{n=0}^{\infty}\frac{(-1)^n}{(2n+1)^2}\exp\left[-\left(n+\frac{1}{2}\right)^2\pi^2\tau\right]\ \sin\left[\left(n+\frac{1}{2}\right)\pi z\right]\right\}. \tag{4.8}$$

In the examples to follow we set $G=-2$.

4.3. *Drift*

Finally, when surface waves of slope ϵ ride on U, they act to effect a mass transport through a Lagrangian drift velocity resulting from an averaged quadratic (i.e. wave–wave and wave–shear) nonlinearity $\mathscr{D}D(z;\alpha)$, where, for two-dimensional monochromatic waves of small amplitude, $\mathscr{D}=\mathfrak{a}^2\omega\mathfrak{K}$.

Downloaded from https://www.cambridge.org/core. IFREMER - Brest, on 15 Jan 2017 at 17:03:33, subject to the Cambridge Core terms of use, available at https://www.cambridge.org/core/terms. https://doi.org/10.1017/jfm.2014.37

Phillips *et al.* (2010) use (1.1) in combination with (3.1) to show (for $s = 1$) that D' takes the general form

$$D' = \frac{1}{2}\,\mathrm{csch}^2\,\alpha\left\{2\alpha\,\sinh\,2\alpha(z+1) + \vartheta\left[2\alpha U''\sinh\,2\alpha(z+1) - \frac{1}{2}[U''' - (U''' + 4\alpha^2 U')\cosh\,2\alpha(z+1)]\right]\right\} \tag{4.9}$$

with the parameter

$$\vartheta = \frac{\epsilon}{2\alpha^{3/2}\sqrt{\mathfrak{g}\,\tanh\,\alpha}}. \tag{4.10}$$

Observe that in the absence of shear, or if $\vartheta \to 0$, that (4.9) relaxes to the well-known Stokes drift (Stokes 1847; Longuet-Higgins 1953). To be precise, the term proportional to $\vartheta = O(\epsilon)$ is asymptotically small relative to the Stokes drift once $\alpha \geqslant O(1)$.

It is also useful to know that in the limit $\alpha \to 0$, we find that the U''' term vanishes leaving

$$D' \sim 2(z+1) + \frac{\epsilon}{\alpha^2\sqrt{\mathfrak{g}}}\left[U''(z+1) + \frac{U'}{2}\right] \tag{4.11}$$

from which we see that $D' \sim 2(z+1)$ if $U' = 0$ or $D' \sim \alpha^{-2}$ if $U' \neq 0$.

4.4. *Numerical formulation*

Our intent is to solve (4.2*a*) subject to (4.4) and (4.5) numerically using the Galerkin method. Details are contained in Phillips & Wu (1994) and Phillips (2001*a*), but briefly the dependent variables $\mathfrak{u}$ and $\mathfrak{w}$ are each expanded in linearly independent, complete sets of basis functions in z that satisfy (4.4) and (4.5) truncated after N terms. The time-dependent coefficients multiplying the basis functions at each order, $\boldsymbol{a}(t)$ say, are unknown. Evaluation of the inner products on (4.2) then leads to a system of $2N$ linear, homogeneous ordinary differential equations (ODEs) of the form

$$\frac{\mathrm{d}\boldsymbol{a}}{\mathrm{d}t} = \boldsymbol{A}(t)\boldsymbol{a}, \tag{4.12}$$

where the elements of the matrix $\boldsymbol{A}(t)$ are known from the inner products. In view of (4.7) and (4.8), however, it is evident that $\boldsymbol{A}(t)$ relaxes to a constant as $t \to \infty$ and the problem reduces to one with constant coefficients. We then expect asymptotic stability to be determined solely by the growth rates, that is eigenvalues, corresponding to the constant matrix $\boldsymbol{A}(\infty)$.

We use Chebyshev polynomials as basis functions as their properties can be exploited by Gaussian quadrature to provide accurate, efficient integration of the inner products. Finally, the eigenvalue problem (4.12) is solved using Lapak with $N = 25$. In limiting cases we accurately recovered the analytical onset values in the case of Cox & Leibovich (1993), as discussed in § 5.1.

5. Results: the limiting case $U' = 1,\ |D'| = 1$

Cox & Leibovich (1993) consider the formation of LC in a surface layer $-1 \leqslant z \leqslant 0$ bounded by a thermocline in the presence of deep-water waves. In order to proceed analytically they restrict attention to waves in the $\alpha \to 0$ limit for which the differential drift, when normalized appropriately, is given by $\lim_{\alpha\to 0} \mathrm{e}^{\alpha z} \sim 1$ throughout the layer.

Downloaded from https://www.cambridge.org/core. IFREMER - Brest, on 15 Jan 2017 at 17:03:33, subject to the Cambridge Core terms of use, available at https://www.cambridge.org/core/terms. https://doi.org/10.1017/jfm.2014.37

This they consider in conjunction with a stress-driven flow (§ 4.2.1) in the limit $\tau \to \infty$ for which U' is likewise unity throughout the layer. We shall ease these restrictions § 6 but for the moment we should like to revisit their case (§ 5.2) and thence consider a simplistic pressure driven flow representative of a current (§ 5.3). First, however, we shall compare the boundary conditions we derived in § 4.1 with their heuristic ones.

5.1. *Comparison with the heuristic boundary conditions of Cox & Leibovich*

Cox & Leibovich (1993) correctly argued that the free-surface boundary conditions are Cauchy, although the precise form is somewhat richer than they foresaw. Specifically, their counterpart to (3.12*a*) on $z = 0$ is

$$\mathfrak{u}' + \gamma_t \mathfrak{u} = 0, \tag{5.1}$$

where γ_t is a positive constant. In fact, as we saw in (4.4*b*), $\mathfrak{u}$ is not premultiplied by a constant but rather by a term which varies with α and l. There is also a difference in sign.

Accordingly, for their boundary conditions on the stream function $\psi = (\mathfrak{w}/l)\sin ly$, they assume

$$\mathfrak{w}'' + \tfrac{1}{2}\gamma_t \mathfrak{w}' = \mathfrak{w} = 0. \tag{5.2}$$

In this instance their sign concurs with ours but again $\mathfrak{w}'$ in (4.4*c*) is premultiplied by a term which varies with α and l. We further note that (5.2) can replicate (4.4*d*) only if $\mathfrak{w} = 0$.

At the bottom of the layer they assume a strong thermocline with boundary conditions $\mathfrak{u}' - \gamma_b \mathfrak{u} = 0$ and $\mathfrak{w}'' - \gamma_b \mathfrak{w}' = \mathfrak{w} = 0$ where γ_b is a positive constant. We do not derive boundary conditions at a thermocline, but for comparative purposes we shall employ their conditions and also Dirichet, as would occur at a rigid boundary.

Finally, since we are dealing with multiple boundary conditions, it is helpful to have a symbol for each. So, since (4.5) are largely Dirichet we denote them by $\mathfrak{D}$; likewise since (5.1) and (5.2) with $\gamma_t = 0$ or $\gamma_b = 0$ are Neumann we denote them by $\mathfrak{N}$. Our remaining conditions are both Cauchy, so we refer to (5.1) and the set (5.2) with $\gamma_t \neq 0$ or $\gamma_b \neq 0$ as $\mathfrak{C}$ and (4.4) as $\mathfrak{P}$. Further, to indicate which is at the free surface $z = 0$ (top) and which is at the bottom $z = -1$ we group them in the order top–bottom. Thus, $\mathfrak{CD}$ means $\mathfrak{C}$ on top and $\mathfrak{D}$ on the bottom.

5.2. *Uniform shear: Cox & Leibovich revisited*

Cox & Leibovich (1993) employ $\mathfrak{NN}$ and then $\mathfrak{CC}$ with, as noted above, $U' = 1$ and $D' = 1$. With the former, in neutrally buoyant conditions, the critical wavenumber l_c is zero, so that the first motions to become linearly unstable occur on the largest horizontal scale available. This occurs when the critical Rayleigh number $\mathcal{R}_c^* = 120$. Note that because of a difference in normalization their Rayleigh number $\mathcal{R}^* = 4\mathcal{R}$. Our calculations concur precisely and we plot $\mathcal{R}^{*1/2}$ in figure 1.

Cox & Leibovich (1993) then employ $\mathfrak{CC}$ with $\gamma_t = 0.06$ and $\gamma_b = 0.28$, these being values they obtained from physical arguments. Our neutral curve likewise recovers theirs and is shown in figure 1. Chini & Leibovich (2003) later considered $\mathfrak{NC}$ (not shown), with which we likewise concur.

Finally to see how our consistent boundary conditions affect the results we include $\mathfrak{PD}$ (with (4.4) in the limit $\alpha \to 0$) to compare with $\mathfrak{CD}$, and $\mathfrak{PC}$ to compare with $\mathfrak{CC}$. As we might expect the ensuing neutral curves are not dissimilar to those of Cox

Downloaded from https://www.cambridge.org/core. IFREMER - Brest, on 15 Jan 2017 at 17:03:33, subject to the Cambridge Core terms of use, available at https://www.cambridge.org/core/terms. https://doi.org/10.1017/jfm.2014.37

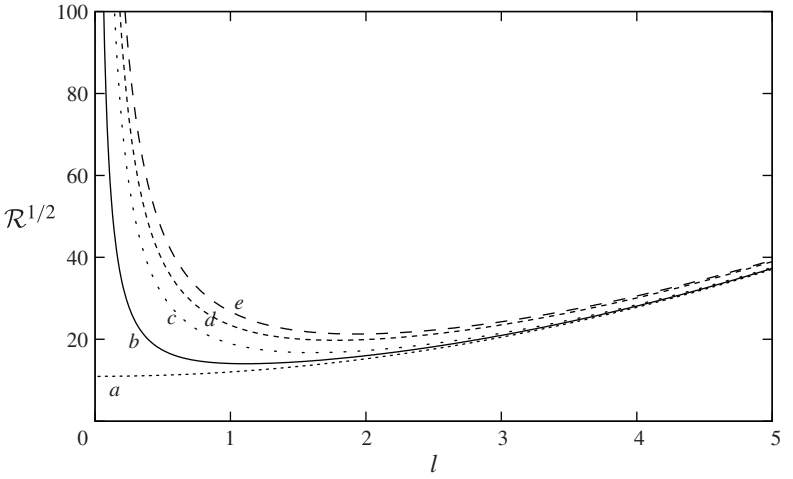

FIGURE 1. Neutral curves for various boundary conditions with uniform gradients of drift and mean velocity with onset values $(l, \mathcal{R}^{*1/2})$ in the limit $\alpha \to 0$: (*a*) $\mathfrak{MM}$, $(0, \sqrt{120})$; (*b*) $\mathfrak{CC}$, (1.111, 14.035) after Cox & Leibovich (1993); (*c*) $\mathfrak{PC}$, (1.610, 16.741); (*d*) $\mathfrak{CD}$, (1.773, 19.763); (*e*) $\mathfrak{PD}$, (1.930, 21.280).

& Leibovich (1993) and are in fact asymptotic to them for large l. From the figure we further see that the curves depict increasingly higher onset numbers $(l_c, \mathcal{R}_c^{*1/2})$ (given in the caption for figure 1) as we progress from $\mathfrak{MM}$ to $\mathfrak{CC}$ and thence to $\mathfrak{PC}$, $\mathfrak{CD}$ and $\mathfrak{PD}$.

5.3. *Non-uniform shear*

Comfortable that our numerics concur with previous work we now proceed with further cases, the first being an idealistic version of a current-like flow. Before proceeding, however, it is useful to review the instability criterion for CL2, which decrees that an inviscid fluid system of infinite depth be stable to the formation of LC if the product $D'U'$ is everywhere negative (Leibovich 1977*b*). This statement gives rise to two questions: first, whether or not the qualifier 'everywhere' conversely requires $D'U'$ be everywhere positive for Langmuir circulation to form and if not, over what fraction of the domain must $D'U'$ be positive? And second, if LC do form when $D'U'$ is not everywhere positive, whether they confine themselves solely to that part of the domain in which $D'U'$ is positive?

To gain insight into these questions we contrive that $D'U'$ be positive over only a portion of the domain: to wit for simplicity we leave $D' = 1$ as before but set $U' = 1$ in $[-1, z^*]$ with $U' = -1$ in $[z^*, 0]$, yielding a crude approximation to a parabolic-like flow. We then investigate the stability of the system.

Interestingly, we find the system is unstable for all $z^* \neq -1$, from which it follows that $D'U'$ *need not* be everywhere positive for LC to form. However, if we take this to the limit where $D'U'$ is positive only at a point (say as $z^* \to -1$) we find that while LC do indeed form, they do so only in the limit $\mathcal{R}^* \to \infty$. That said, onset $\mathcal{R}^*$ plummets to realizable values when $D'U'$ is positive over $0 < 1 + z^* \ll 1$. In summary, then, instability is assured when $D'U'$ is positive at a point and realized easily when $D'U'$ is positive over more than a point.

Downloaded from https://www.cambridge.org/core. IFREMER - Brest, on 15 Jan 2017 at 17:03:33, subject to the Cambridge Core terms of use, available at https://www.cambridge.org/core/terms. https://doi.org/10.1017/jfm.2014.37

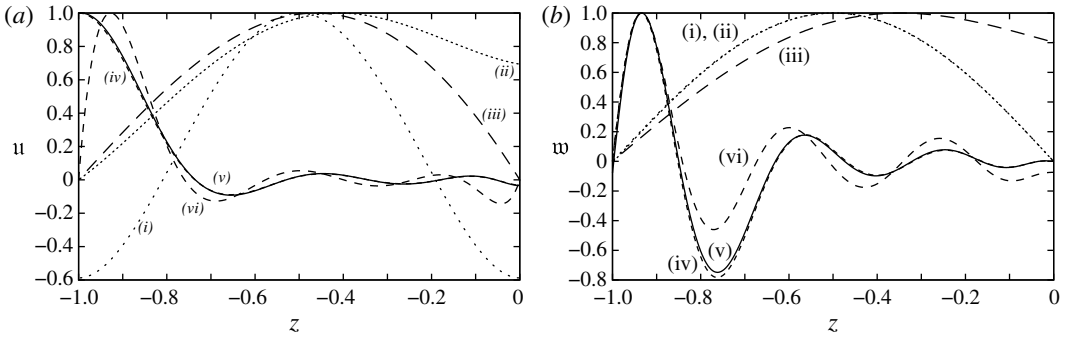

FIGURE 2. Eigenfunctions for (*a*) $\mathfrak{u}$ and (*b*) $\mathfrak{w}$ for various boundary conditions in uniform shear, (i) $\mathfrak{NN}_A$, (ii) $\mathfrak{CC}_A$ and (iii) $\mathfrak{CC}_A$, and non-uniform shear, (iv) $\mathfrak{NN}_B$, (v) $\mathfrak{CC}_B$ and (vi) $\mathfrak{CC}_B$. Here $l \to 0$ for $\mathfrak{N}$ boundary conditions and $l = 1$ otherwise.

But are LC confined solely to the region in which $D'U' > 0$? To resolve this we turn to the eigenfunctions (normalized to unity), shown in figure 2. These were evaluated in the limit $l \to 0$ for $\mathfrak{N}$ boundary conditions and at $l = 1$ otherwise. For comparison we include eigenfunctions for the case with uniform shear (subscript '*A*') and those for non-uniform shear with, for illustration, $z^* = -0.9$ (subscript '*B*').

Looking first at the results for uniform shear (figure 2 curves (i), (ii) and (iii)) we note that our numerics precisely recover the analytical solutions given by Cox & Leibovich (1993) for $\mathfrak{NN}_A$ (i). On comparing these with $\mathfrak{CC}_A$ (ii) we see that while $\mathfrak{w}$ is essentially unchanged from its $\mathfrak{NN}_A$ counterpart, the eigenfunction $\mathfrak{u}$ is somewhat different, depicting a perturbation flow at the free surface as expected. Finally, we noted earlier that while the perturbation flow $\mathfrak{u}$ on $z = 0$ vanishes as $\alpha \to 0$ with $\mathfrak{PD}$ boundary conditions, that is not the case for $\mathfrak{w}$ and both are reflected in the eigenfunctions as we see in (iii).

Turning now to non-uniform shear (figure 2 curves (iv), (v) and (vi)) we observe that the eigenfunctions for $\mathfrak{u}$ (figure 2(*a*)) depict little action in the upper part of the layer with a maximum at ($\mathfrak{NN}_B$, $\mathfrak{CC}_B$ i.e. curves (iv) and (v)) or near ($\mathfrak{PD}_B$, curve (vi)) the bottom. Their counterparts for $\mathfrak{w}$ likewise peak near the bottom and $\mathfrak{NN}_B$ and $\mathfrak{CC}_B$ are virtually identical, with $\mathfrak{PD}_B$ not dissimilar. That said there are three key points to note.

First, the eigenfunctions for $\mathfrak{w}$ (or streamfunction ψ) depict multiple zeros and thus a change of sign in the interior. This means the LC do not form in a single layer, which is the expectation (and the case in uniform shear), but rather form a stacked array. Second, the intensity of the LC diminish with distance from the wall. Third, and of particular importance, the LC are not confined to the region in which $D'U' > 0$.

To the best of the authors' knowledge, the notion of stacked Langmuir circulation has not previously been reported but it is of key interest from the viewpoint to sediment transport from the ocean floor. More profound is that Langmuir circulation excited as a consequence of the requirement $D'U' > 0$ are not confined to the region in which $D'U'$ is positive, a feature which may partially explain why the ocean mixed layer can exceed the depth to which the drift extends.

Of course our findings may be an artifact of the simplistic velocity and drift distributions we have employed here and so to find out we now consider the dynamically consistent drift and shear distributions (Phillips *et al.* 2010) reported for shallow-water waves propagating on a moderate shear flow.

Downloaded from https://www.cambridge.org/core. IFREMER - Brest, on 15 Jan 2017 at 17:03:33, subject to the Cambridge Core terms of use, available at https://www.cambridge.org/core/terms. https://doi.org/10.1017/jfm.2014.37

6. Results: the general case

We now ease the restrictions imposed in § 5 and consider a broad range of water waves (from shallow to deep) of constant slope $\epsilon = 0.1$ in sheared layers, bounded by a rigid bottom. To that end we employ the velocity profiles and drift distributions derived by Phillips *et al.* (2010). Further, since it is useful to discuss the results from the viewpoint of a reference and specifically since we are interested in the role of drift rather than Stokes drift, we utilize analogous results based upon the Stokes drift as the reference, noting (see § 4.3) that the drift is asymptotic to the Stokes drift for $\alpha \geqslant O(1)$. That said the ensuing reference results are affected by α, which appears both in the Stokes drift and the boundary conditions; and by τ, which determines U. To proceed, therefore, we choose as a reference the neutral curve for which $\tau \to \infty$ and $\vartheta = 0$, with α set to the same value as the other curves under discussion.

6.1. $\mathfrak{NN}$ *boundary conditions*

Concordant with our approach in § 5, we begin with $\mathfrak{NN}$ boundary conditions but now consider non-uniform distributions of shear and differential drift. To that end we consider neutral curves for $\mathcal{R}^{1/2}$, first with l at constant α (in figure 3(*a, b*)) and then with α at constant l (in figure 4(*a, b*)). In each case we also vary τ, but only show that variation in figure 3(*a, b*) where we consider events in the limit $\alpha \to 0$ (in fact $\alpha = 0.001$).

Looking first at the reference curve in figure 3(*a*) (shown for illustrative purposes $\times 10^{-2}$) we see, as Cox & Leibovich (1993) found, that the least-stable mode occurs always at zero wavenumber in shear-driven flows (figure 3(*a*)). On the other hand, the least-stable mode occurs for non-zero values of l in pressure-driven flows (figure 3(*b*)), typically at values of about three or larger. This result is important because it means that stress-free or $\mathfrak{NN}$ conditions, long thought to be inappropriate to the class of equations (2.9) on the finite domain can, in some circumstances, be physically meaningful boundary conditions.

Observe too that the results are strongly dependent on τ. Looking first at figure 3(*a*) we see that, relative to the reference case, the influence of shear acts to significantly lower the value of $\mathcal{R}$ at which onset occurs, the minimal occurring in the limit $\tau \to \infty$. In pressure-driven flow on the other hand (figure 3(*b*)), $\mathcal{R}$ can be higher or lower than the reference level, with again the minimal value occurring in the limit $\tau \to \infty$.

But what of the role of α? Before looking at specific cases, we note from (4.2*c*) and (4.9) that onset is to be expected as $\mathcal{R} \to 0$ in the limit $\alpha \to 0$ for any $U' \neq 0$ and necessarily increases as α increases, provided of course that ϵ does not go to zero faster than α^2. That said, the value of $\mathcal{R}$ at which onset occurs is ultimately asymptotic to the reference curve which acts to bound it from above for shear-driven flows (since they are destabilizing to the formation of LC) and from below for pressure-driven flows (which are stabilizing) as we see in figure 4, where we plot two cases representative of the least-stable limits in l, namely $l \to 0$ and $l = 3$ for $\tau \to \infty$. This further necessitates that $\mathcal{R}$ first climb (with increasing α) through the reference level, as we see in figure 4(*b*). Of course the same behaviour occurs in figure 4(*a*) as well, but it is hidden because of its high gradient in the vicinity of $\alpha \to 0$. Also beyond the bounds of figure 4(*a*) is the peak in the onset value of $\mathcal{R}$, a feature which is shown in figure 4(*b*). Since l is larger in figure 4(*b*) (with τ constant) we might infer that the peak in $\mathcal{R}$ decreases with increasing l, and that is in fact the case. Concordantly, on fixing l and varying τ we likewise find the peak in $\mathcal{R}$ diminishes with τ and reaches its lowest value in the limit $\tau \to \infty$.

Downloaded from https://www.cambridge.org/core. IFREMER - Brest, on 15 Jan 2017 at 17:03:33, subject to the Cambridge Core terms of use, available at https://www.cambridge.org/core/terms. https://doi.org/10.1017/jfm.2014.37

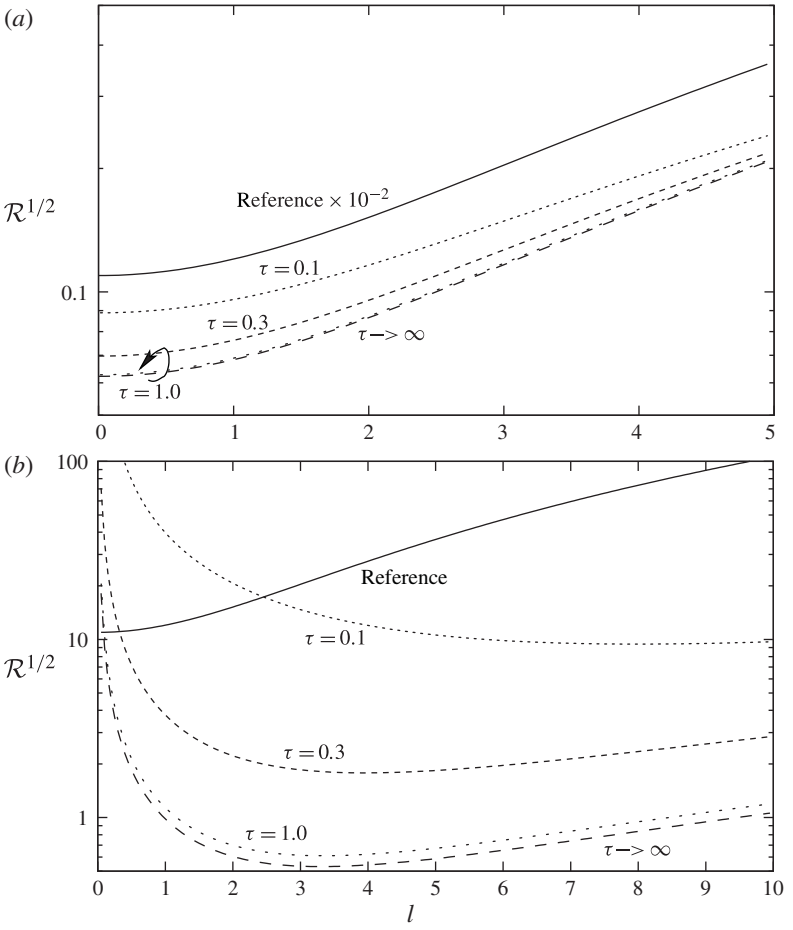

FIGURE 3. Neutral curves of $\mathcal{R}^{1/2}$ against l for various τ in the limit $\alpha \to 0$ for $\mathfrak{MM}$ boundary conditions: (*a*) shear driven; (*b*) pressure driven.

6.2. $\mathfrak{PD}$ *boundary conditions*

Consider now the case in which we impose (4.3) and (4.4), i.e. $\mathfrak{P}$ boundary conditions, at the free surface and no slip, i.e. $\mathfrak{D}$ at the sea floor.

As above we first plot onset $\mathcal{R}$ against l at various τ (figure 5) although here at the physically realizable $\alpha = 0.1$. Looking first at the shear-driven case (figure 5(*a*)) we observe, in accord with our findings above, that $\mathcal{R}$ is always lower than the reference curve. Observe too that $\mathcal{R}$ diminishes with increasing τ and that critical values occur for $\mathcal{R}_c = 6.847$ at $l_c = 1.492$ in the limit $\tau \to \infty$; note also that l_c is essentially independent of τ.

Neutral curves for the pressure-driven case (figure 5(*b*)), on the other hand, depict two distinct forms. The first is typified by the reference curve which has a minimum at about $l = 2$ and is emulated by our curve at $\tau = 0.1$, albeit at higher $\mathcal{R}$. The second form emerges as τ increases through 0.2 where the neutral curve then highlights two local minima. Initially $\mathcal{R}_c$ is lowest at the minima with the largest l. But that becomes less the case as τ increases, to the point that for the least-stable case $\tau \to \infty$, critical $\mathcal{R}$ is much the same at each l, which occur near $l \approx 0.04$ and $l \approx 4$. Immediate

Downloaded from https://www.cambridge.org/core. IFREMER - Brest, on 15 Jan 2017 at 17:03:33, subject to the Cambridge Core terms of use, available at https://www.cambridge.org/core/terms. https://doi.org/10.1017/jfm.2014.37

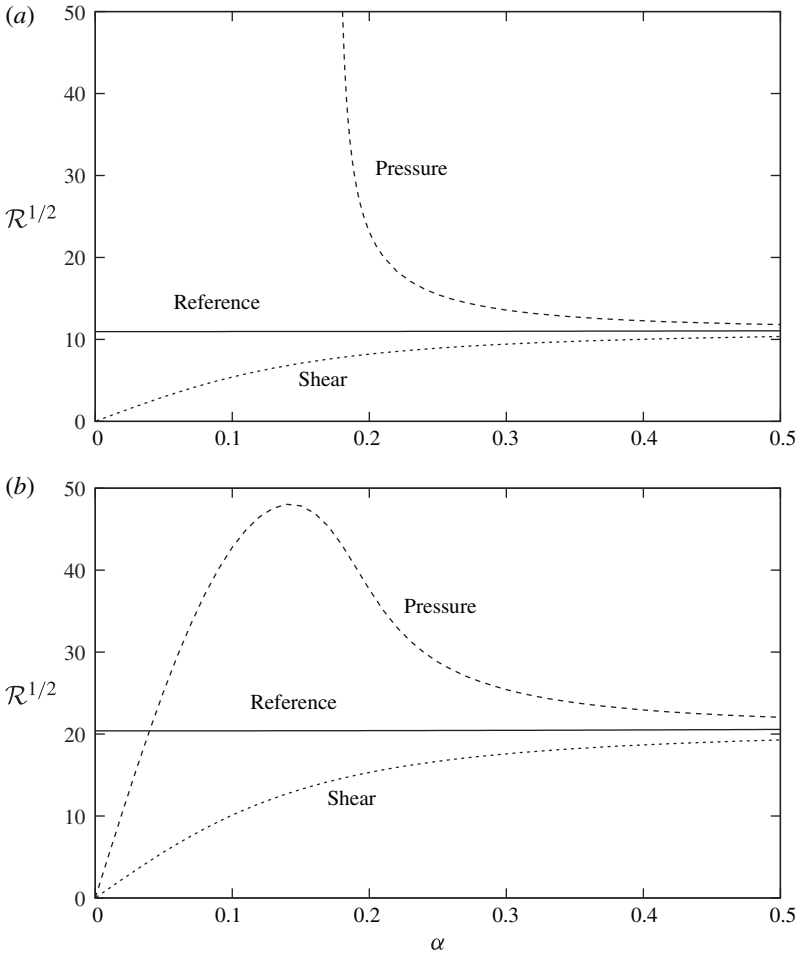

FIGURE 4. Neutral curves of $\mathcal{R}^{1/2}$ against α as $\tau \to \infty$ for $\mathfrak{MM}$ boundary conditions in shear- and pressure-driven flow: (*a*) in the limit $l \to 0$ and (*b*) at $l = 3$.

questions are what is the structure of the LC at each l and whether one spacing is preferred over the other? To answer the former we look at the eigenfunctions at each spacing, while for the latter we look at the growth rates at each spacing.

The eigenfunctions for $\mathfrak{u}$ and $\mathfrak{w}$ at the least-stable $(\mathcal{R}_c,\ l_c)$ for shear- and pressure-driven flow are shown in figure 6, where we see that the structure can vary significantly from case to case. Specifically one cell fills the layer in shear-driven flow with the axial perturbation reaching its peak midway through the layer, much as in the model case in § 5.2. In pressure-driven flows, on the other hand, we observe two layers of LC at $l = 4$ with the stronger cell at the ocean floor and noticeably weaker cell near the ocean surface. This is so for all τ with $l > 0.3$. Once $\tau > 0.2$, however, a second structure emerges for $l < 0.3$ in which just one cell fills the layer, albeit with a $\mathfrak{u}$ component vastly different from its shear-driven counterpart.

Now there is little change in U' as τ increases through 0.2, but there are significant changes in D', in that it changes sign in the upper part of the layer, rendering $D'U' < 0$ there. This phenomenon concurs with that observed in § 5.2 where we further found

Downloaded from https://www.cambridge.org/core. IFREMER - Brest, on 15 Jan 2017 at 17:03:33, subject to the Cambridge Core terms of use, available at https://www.cambridge.org/core/terms. https://doi.org/10.1017/jfm.2014.37

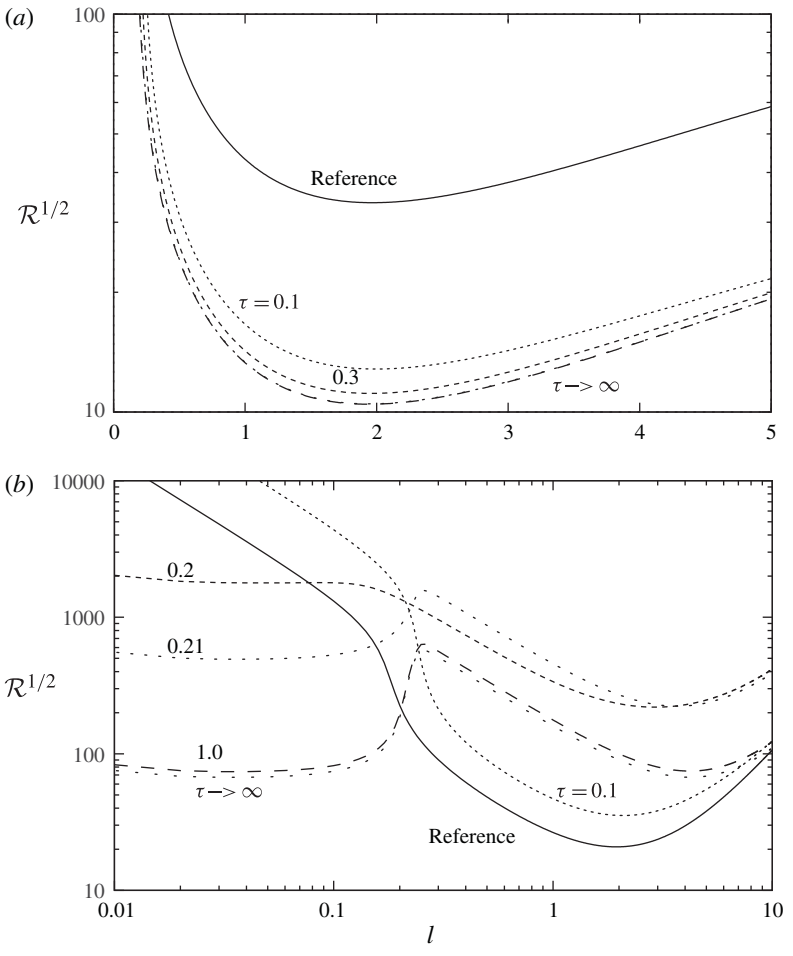

FIGURE 5. Neutral curves of $\mathcal{R}^{1/2}$ against l at $\alpha = 0.1$ for various τ with $\mathfrak{PD}$ boundary conditions: (*a*) shear-driven flow; (*b*) pressure-driven flow.

that LC will form whenever $D'U'$ is positive over some portion of the domain. But why multiple cells, why not just one in the region in which $D'U' > 0$? The simple answer would appear to be one of kinematics, in that the instability gives rise to and drives the lower dominant cells and that continuity of velocity necessitates they in turn drive those above. Contour plots of $\mathfrak{w}$ for a single and double layer of cells are given in figure 7. In viewing them note that, as discussed in § 3.1, a Lagrangian average of the location of the free surface need not occur at $z = 0$ and thus that $\mathfrak{w}$ need not be zero on $z = 0$, which is why only some streamlines in figure 7(*a*) are closed.

Finally, of particular interest is the role of α, and to build our understanding of it we begin by looking at the variation of onset $\mathcal{R}^{1/2}$ with α for the least-stable case $\tau \to \infty$ at a typical l, say $l = 1$ as shown in figure 8. Not surprisingly $\mathcal{R}^{1/2}$ here emulates that in figure 4 in which the neutral curves increase with α from zero and quickly ($\alpha < 1$) asymptote to the reference curve (for which $\mathcal{R}$ is not zero at $\alpha = 0$). Of course of particular interest is the variation of l_c with α, but rather than directly plotting that, and because of the occurrence of two local minima in l, we first plot onset $\mathcal{R}^{1/2}$ against l as in figure 5, although here at various values of α with τ constant,

Downloaded from https://www.cambridge.org/core. IFREMER - Brest, on 15 Jan 2017 at 17:03:33, subject to the Cambridge Core terms of use, available at https://www.cambridge.org/core/terms. https://doi.org/10.1017/jfm.2014.37

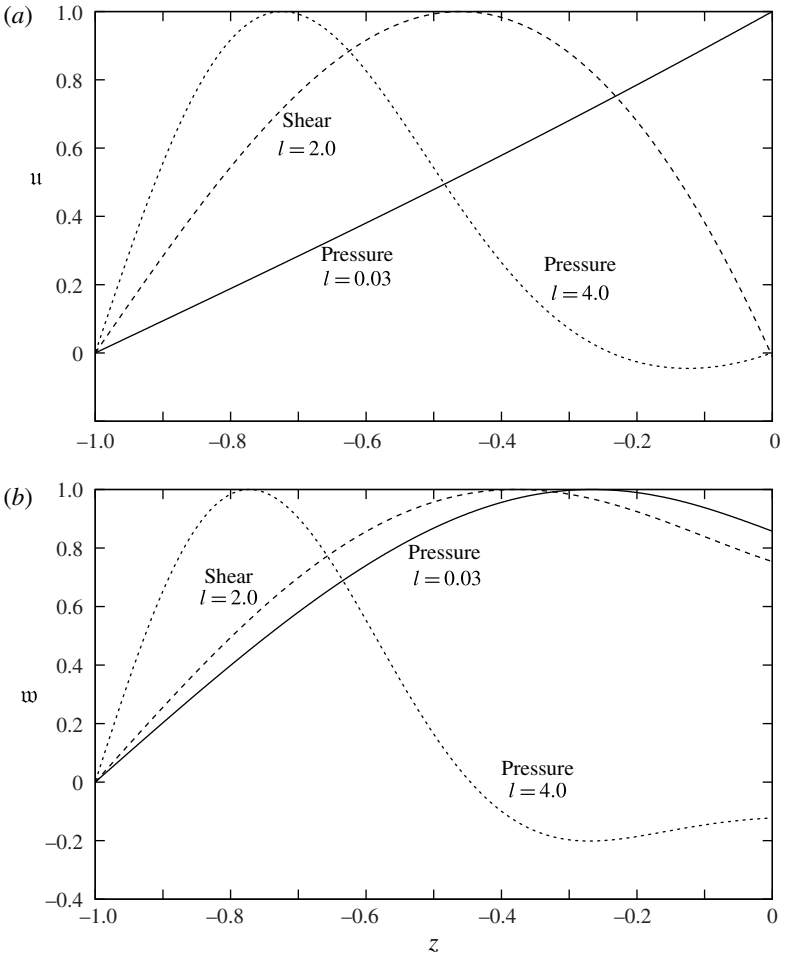

FIGURE 6. Eigenfunctions for (*a*) $\mathfrak{u}$ and (*b*) $\mathfrak{w}$ near critical ($\mathcal{R}$, l) in shear- and pressure-driven flow with $\mathfrak{PD}$ boundary conditions for $\alpha = 0.1$ and $\tau \to \infty$.

specifically $\tau \to \infty$, figure 9. Here we see two local minima for $\alpha < 0.2$ and thus expect two branches on a plot of l_c against α. In fact, in figure 10 we plot $L = 2\pi/l_c$, that is the windrow spacing (two cells) to depth ratio, which allows direct comparison with observation.

Looking first to the branches at the bottom of the figure we see that the aspect ratio of the cells ranges from 1.5 to 3, values completely in accord with deep-water ocean observations (Smith *et al.* 1987; Smith 1992) and those for small-aspect-ratio cells commonly observed in coastal waters (Marmorino *et al.* 2005). This is the case for both shear- and pressure-driven flows. Note too that although the spacing is different for sufficiently small α, it is independent of details of the underlying flow once $\alpha > 0.2$. The upper branch on the other hand is solely for pressure-driven flow for $\alpha < 0.2$. Here we find that L is at least 40, a value well beyond the value of around 10 reported by Hunter & Hill (1980) and Marmorino *et al.* (2005).

But which cells are more likely in pressure-driven flow with $\alpha < 0.2$: highly elongated cells or roughly round cells? To answer that we look at the growth rates.

Downloaded from https://www.cambridge.org/core. IFREMER - Brest, on 15 Jan 2017 at 17:03:33, subject to the Cambridge Core terms of use, available at https://www.cambridge.org/core/terms. https://doi.org/10.1017/jfm.2014.37

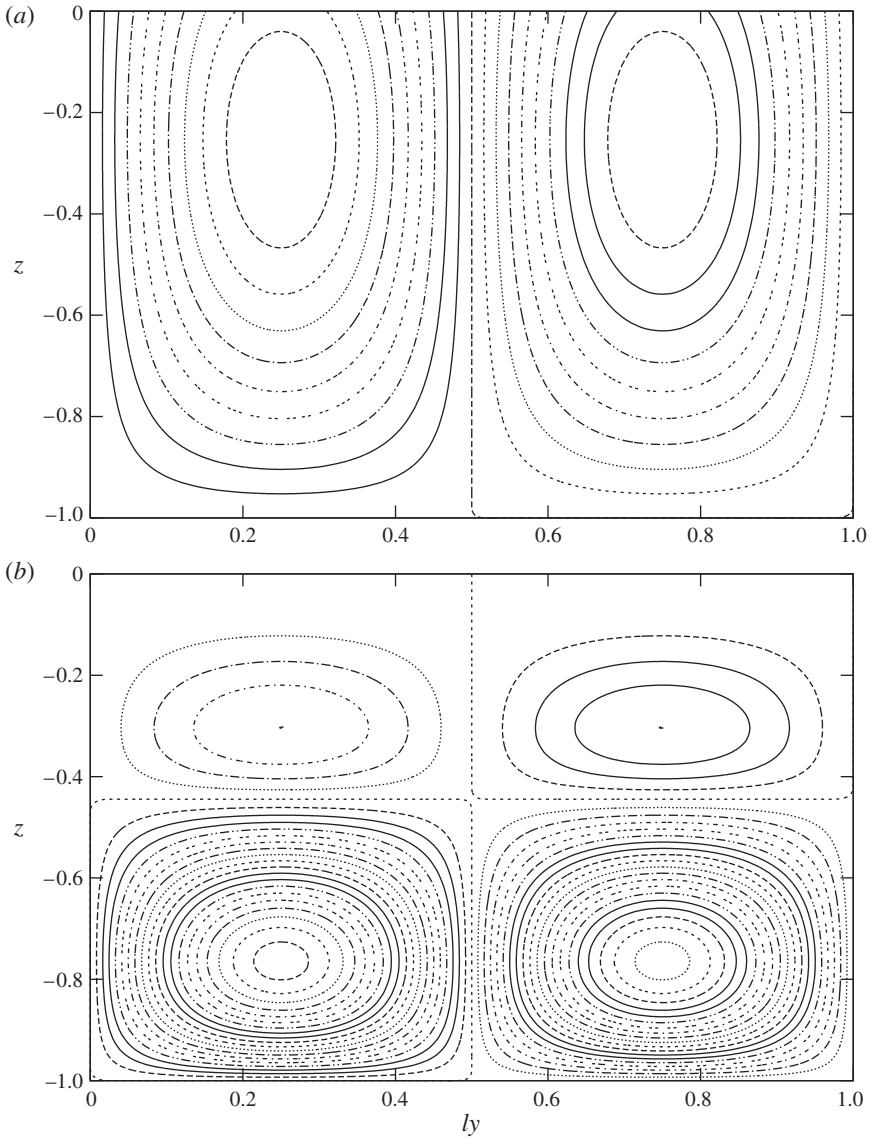

FIGURE 7. Contours of $\mathfrak{w} \propto \psi$ for pressure-driven flow with $\mathfrak{PD}$ boundary conditions for $\alpha = 0.1$ and $\tau \to \infty$ at (*a*) $l = 0.03$ and (*b*) $l = 4$.

Curiously they differ by a factor of less than two, with the growth rate for the large-aspect-ratio cells being higher. This suggests that both are likely present at any time which would, in turn, affect any windrows and thus observed spacing.

7. Discussion

Because differences in the mean shear affect the differential drift in shallow-water waves and because the relationship between them underlies the CL2 instability criterion to LC, Phillips *et al.* (2010) infer that LC first form near the free surface in Couette-like shear-driven flow (and grow downwards, top down) and near the ocean

Downloaded from https://www.cambridge.org/core. IFREMER - Brest, on 15 Jan 2017 at 17:03:33, subject to the Cambridge Core terms of use, available at https://www.cambridge.org/core/terms. https://doi.org/10.1017/jfm.2014.37

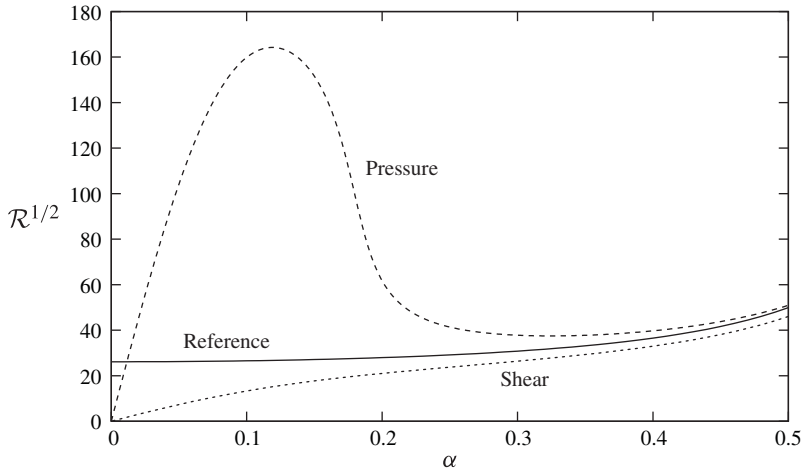

FIGURE 8. Neutral curves of $\mathcal{R}^{1/2}$ against α for $\tau \to \infty$ at $l = 1.0$ for shear- and pressure-driven flow with $\mathfrak{PD}$ boundary conditions.

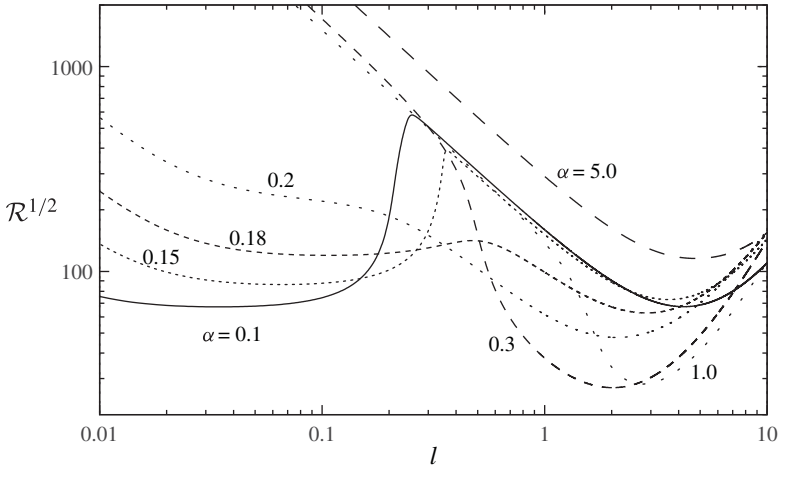

FIGURE 9. Neutral curves of $\mathcal{R}^{1/2}$ against l at various α with $\tau \to \infty$ for pressure-driven flow with $\mathfrak{PD}$ boundary conditions.

floor (and grow upwards, bottom up) in Poiseuille-like pressure-driven flows. Our findings here largely endorse their conjecture and further bring to light the presence of multiple layers of LC in the bottom-up situation. Interestingly when this occurs, the layers extend into a region of flow not satisfied by the CL2 instability criterion. This should not be interpreted to mean the criterion is violated but rather that LC so formed by the instability can, as a dynamic consequence, induce and drive coupled LC in a contiguous region of rotational flow. Thus, in addition to a single layer of LC spanning the entire water column in the sense reported by Gargett *et al.* (2004) as Langmuir supercells, they can likewise effectively mix and transport sediment, etc., as a stacked array. We note that this is not the same as the discrete spectrum of Langmuir cells which combine to form Langmuir turbulence and in fact of particular

Downloaded from https://www.cambridge.org/core. IFREMER - Brest, on 15 Jan 2017 at 17:03:33, subject to the Cambridge Core terms of use, available at https://www.cambridge.org/core/terms. https://doi.org/10.1017/jfm.2014.37

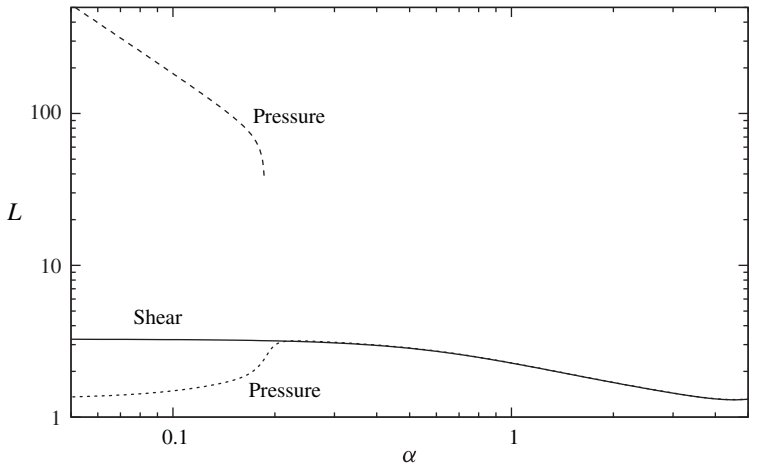

FIGURE 10. Windrow spacing (two cells) namely $2\pi/l_c$ against α for $\tau \to \infty$ with $\mathfrak{PD}$ boundary conditions in both shear- and pressure-driven flow.

interest would be an analogous large eddy simulation calculation of the cases studied here.

Clear too from our study is the finding that omission of the shear-related component of drift (that is use of the Stokes drift alone), can yield very misleading onset results particularly in pressure-driven flows. Of course this finding is most relevant in shallow water waves in the inner coastal region and diminishes once $\alpha \geqslant O(1)$.

Finally, with regard to boundary conditions, we found that $\mathfrak{MM}$ conditions, long thought to yield non-physical results when applied to flows on the finite domain, can be meaningful in the sense that they act to realize finite spacing, but only in pressure-driven flows. On the other hand the presence of a small perturbations in shear stress on the free surface, as occur with the consistent $\mathfrak{PD}$ boundary conditions derived herein, act to ensure finite onset spacing irrespective of the details of the primary shear flow. Furthermore, in pressure-driven flow these conditions admit two preferred spacings, one well in accord with observations for small-aspect-ratio LC and the other well in excess of observed large-aspect-ratio LC.

Acknowledgements

We would like to thank Sergey Suslov for his interest and helpful comments. This work was supported by the US National Science Foundation through grant OCE-0116921, by the Australian Research Council through grants LP0883888 and DP1093517 and by the Taiwan National Science Council through grant NSC-101-2628-E032-003-MY3.

REFERENCES

ANDREWS, D. G. & MCINTYRE, M. E. 1978 An exact theory of nonlinear waves on a Lagrangian-mean flow. *J. Fluid Mech.* **89**, 609–646.

BABANIN, A. V., GANOPOLSKI, A. & PHILLIPS, W. R. C. 2009 Wave-induced upper-ocean mixing in a climate model of intermediate complexity. *Ocean Model.* **29**, 189–197.

BLONDEAUX, P., BROCCHINI, M. & VITTORI, G. 2002 Sea waves and mass transport on a sloping beach. *Proc. R. Soc. Lond.* A **458**, 2053–2082.

Downloaded from https://www.cambridge.org/core. IFREMER - Brest, on 15 Jan 2017 at 17:03:33, subject to the Cambridge Core terms of use, available at https://www.cambridge.org/core/terms. https://doi.org/10.1017/jfm.2014.37

CHAPMAN, C. J., CHILDRESS, S. & PROCTOR, M. R. E. 1980 Long wavelength thermal convection between nonconducting boundaries. *Earth Planet. Sci. Lett.* **51**, 362–369.

CHAPMAN, C. J. & PROCTOR, M. R. E. 1980 Nonlinear Rayleigh–Benard convection between poorly conducting boundaries. *J. Fluid Mech.* **101**, 759–782.

CHINI, G. P. & LEIBOVICH, S. 2003 Resonant Langmuir-circulation–internal-wave interaction. Part 1. Internal wave reflection. *J. Fluid Mech.* **495**, 35–55.

CHINI, G. P. & LEIBOVICH, S. 2005 Resonant Langmuir-circulation–internal-wave interaction. Part 2. Langmuir circulation instability. *J. Fluid Mech.* **524**, 99–120.

COX, S. & LEIBOVICH, S. 1993 Langmuir circulations in a surface layer bounded by a strong thermocline. *J. Phys. Oceanogr.* **23**, 1330–1345.

CRAIK, A. D. D. 1977 The generation of Langmuir circulations by an instability mechanism. *J. Fluid Mech.* **81**, 209–223.

CRAIK, A. D. D. 1982 Wave induced longitudinal-vortex instability in shear flows. *J. Fluid Mech.* **125**, 37–52.

CRAIK, A. D. D. & LEIBOVICH, S. 1976 A rational model for Langmuir circulations. *J. Fluid Mech.* **73**, 401–426.

GARGETT, A., WELLS, J., TEJADA-MARTINEZ, A. E. & GROSCH, C. E. 2004 Langmuir supercells: a mechanism for sediment resuspension and transport in shallow seas. *Science* **306**, 1925–1928.

HUNTER, R. & HILL, G. W. 1980 Nearshore current pattern off South Texas—an interpretation from aerial photographs. *Remote Sens. Environ.* **10**, 115–134.

LANGMUIR, I. 1938 Surface motion of water induced by wind. *Science* **87**, 119–123.

LEIBOVICH, S. 1977 Convective instability of stably stratified water in the ocean. *J. Fluid Mech.* **82**, 561–585.

LEIBOVICH, S. 1980 On wave-current interaction theories of Langmuir circulation. *J. Fluid Mech.* **99**, 715–724.

LEIBOVICH, S. 1983 The form and dynamics of Langmuir circulations. *Annu. Rev. Fluid Mech.* **15**, 391–427.

LONGUET-HIGGINS, M. S. 1953 Mass transport in water waves. *Phil. Trans. R. Soc. Lond.* **245**, 535–581.

MARMORINO, G. O., SMITH, G. B. & LINDEMANN, G. J. 2004 Infrared imagery of ocean internal waves. *Geophys. Res. Lett.* **31**, L11309.

MARMORINO, G. O., SMITH, G. B. & LINDEMANN, G. J. 2005 Infrared imagery of large-aspect-ratio Langmuir circulation. *Cont. Shelf Res.* **25**, 1–6.

MARTINAT, G., XU, Y., GROSCH, C. & TEJADA-MARTINEZ, A. 2011 LES of turbulent surface shear stress and pressure-gradient-driven flow on shallow continental shelves. *Ocean Dyn.* **61**, 1369–1390.

MCINTYRE, M. & NORTON, W. 1990 Dissipative wave-mean interactions and the transport of vorticity or potential vorticity. *J. Fluid Mech.* **212**, 403–435.

MCLEISH, W. 1968 On mechanisms of wind-slick generation. *Deep-Sea Res.* **15**, 461–469.

MELVILLE, W. K., SHEAR, R. & VERON, F. 1998 Laboratory measurements of the generation and evolution of Langmuir circulations. *J. Fluid Mech.* **364**, 31–58.

MOROZ, I. M. & LEIBOVICH, S. 1985 Oscillatory and competing instabilites in a nonlinear model for Langmuir circulations. *Phys. Fluids* **28**, 2050–2061.

NIELD, D. A. 1967 The thermohaline Rayleigh–Jeffreys problem. *J. Fluid Mech.* **29**, 545–558.

PHILLIPS, W. R. C. 1998 Finite amplitude rotational waves in viscous shear flows. *Stud. Appl. Maths* **101**, 23–47.

PHILLIPS, W. R. C. 2001*a* On an instability to Langmuir circulations and the role of Prandtl and Richardson numbers. *J. Fluid Mech.* **442**, 335–358.

PHILLIPS, W. R. C. 2001*b* On the pseudomomentum and generalized Stokes drift in a spectrum of rotational waves. *J. Fluid Mech.* **430**, 209–220.

PHILLIPS, W. R. C. 2002 Langmuir circulations beneath growing or decaying surface waves. *J. Fluid Mech.* **469**, 317–342.

PHILLIPS, W. R. C. 2003 Langmuir circulations. In *Wind-Over-Waves II: Forecasting and Fundamentals of Applications* (ed. S. Sajjadi & J. Hunt), pp. 157–167. Horwood Pub.

Downloaded from https://www.cambridge.org/core. IFREMER - Brest, on 15 Jan 2017 at 17:03:33, subject to the Cambridge Core terms of use, available at https://www.cambridge.org/core/terms. https://doi.org/10.1017/jfm.2014.37

PHILLIPS, W. R. C. 2005 On the spacing of Langmuir circulation in strong shear. *J. Fluid Mech.* **525**, 215–236.

PHILLIPS, W. R. C., DAI, A. & TJAN, K. 2010 On Lagrangian drift in shallow-water waves on moderate shear. *J. Fluid Mech.* **660**, 221–239.

PHILLIPS, W. R. C. & SHEN, Q. 1996 A family of wave-mean shear interactions and their instability to longitudinal vortex form. *Stud. Appl. Maths* **96**, 143–161.

PHILLIPS, W. R. C. & WU, Z. 1994 On the instability of wave-catalysed longitudinal vortices in strong shear. *J. Fluid Mech.* **272**, 235–254.

PHILLIPS, W. R. C., WU, Z. & LUMLEY, J. 1996 On the formation of longitudinal vortices in turbulent boundary layers over wavy terrain. *J. Fluid Mech.* **326**, 321–341.

PLUEDDEMANN, A., SMITH, J., FARMER, D., WELLER, R., CRAWFORD, W., PINKEL, R., VAGLE, S. & GNANADESIKAN, A. 1996 Structure and variability of Langmuir circulation during the surface waves processes program. *J. Geophys. Res.* **21**, 85–102.

SMITH, J., PINKEL, R. & WELLER, R. A. 1987 Velocity structure in the mixed layer during mildex. *J. Phys. Oceanogr.* **17**, 425–439.

SMITH, J. A. 1992 Observed growth of Langmuir circulation. *J. Geophys. Res.* **97**, 5651–5664.

SPARROW, E. M., GOLDSTEIN, R. J. & JONSSON, V. K. 1964 Thermal instability in a horizontal fluid layer: effect of boundary conditions and non-linear temperature profile. *J. Fluid Mech.* **18**, 513–528.

STOKES, G. G. 1847 On the theory of oscillatory waves. *Trans. Camb. Phil. Soc.* **8**, 441–455.

TEJADA-MARTINEZ, A. & GROSCH, C. 2007 Langmuir turbulence in shallow water. Part 2. Large-eddy simulation. *J. Fluid Mech.* **576**, 27–61.

THORPE, S. 2004 Langmuir circulation. *Annu. Rev. Fluid Mech.* **36**, 55–79.

VERON, F. & MELVILLE, W. K. 2001 Experiments on the stability and transition of wind-driven water surfaces. *J. Fluid Mech.* **446**, 25–65.

WEBER, J. & GHAFFARI, P. 2009 Mass transport in the Stokes edge wave. *J. Mar. Res.* **67**, 213–224.

Downloaded from https://www.cambridge.org/core. IFREMER - Brest, on 15 Jan 2017 at 17:03:33, subject to the Cambridge Core terms of use, available at https://www.cambridge.org/core/terms. https://doi.org/10.1017/jfm.2014.37